Inorganic Chemistry
Cite This: Inorg. Chem. XXXX, XXX, XXX–XXX
Forum Article
pubs.acs.org/IC

Implementing f-Block Metal Ions in Medicine: Tuning the Size Selectivity of Expanded Macrocycles

Nikki A. Thiele,[†,§] Joshua J. Woods,[†,‡,§] and Justin J. Wilson*[,†]

[†]Department of Chemistry and Chemical Biology and [‡]Robert F. Smith School for Chemical and Biomolecular Engineering, Cornell University, Ithaca, New York 14853, United States

Supporting Information

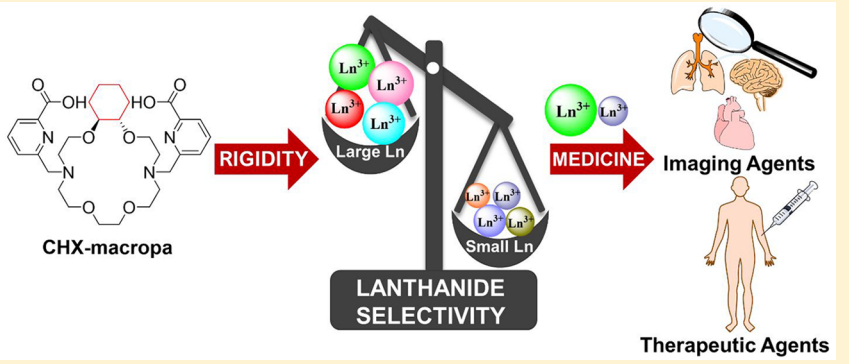

ABSTRACT: The f-block elements, which comprise both the lanthanide and actinide series, possess interesting spectroscopic, magnetic, and nuclear properties that make them uniquely suited for a range of biomedical applications. In this Forum Article, we provide a concise overview on the different ways that these elements are employed in medicine, highlighting their dual implementation in both diagnostic and therapeutic applications. A key requirement for the use of these labile metal ions in medicine is a suitable chelating agent that controls their in vivo biodistribution. Toward this goal, we also report our research describing the synthesis and characterization of a rigid 18-membered macrocycle called CHX-macropa, an analogue of the previously reported nonrigid ligand macropa (*J. Am. Chem. Soc.* **2009**, *131*, 3331). The lanthanide coordination chemistry of CHX-macropa is explored in detail by pH potentiometry and density functional theory (DFT) calculations. These studies reveal that CHX-macropa exhibits an enhanced thermodynamic selectivity for large over small lanthanides in comparison to its nonrigid analogue macropa. DFT calculations suggest that a key factor in the enhanced selectivity of this ligand for the large f-block ions is its rigid macrocyclic core, which cannot adequately distort to interact effectively with small ions. On the basis of its high affinity for large f-block ions, the design strategies implemented in CHX-macropa may be valuable for applying these elements in the diagnosis or treatment of disease.

INTRODUCTION

The U.S. Food and Drug Administration (FDA) approval of the simple coordination compound *cis*-diamminedichloridoplatinum(II), or cisplatin, in 1978 for the treatment of cancer was a significant milestone in the field of medicinal chemistry.[1,2] The demonstration of the efficacy of this compound in a wide range of cancer types was key in supporting the idea that metal-containing compounds may have significant value in the development of new medicines.[3,4] Since then, the field of metals in medicine has dramatically expanded. Researchers have capitalized on the unique chemical and physical properties afforded by metal centers that are otherwise inaccessible by conventional organic molecules to develop an extensive library of novel medicinal agents comprising elements spanning the Periodic Table.[5] Underscoring the diverse utility of metals in medicine, dozens of metallodrugs are currently employed in the diagnosis, imaging, and treatment of a wide range of human diseases and ailments, including cancer, heart disease, infection, arthritis, and gastrointestinal disease.[6,7]

Lanthanides in Medicine. Among the different classes of metal ions in the Periodic Table, lanthanides (Ln), comprising the 15 4f elements, have played a central role in both diagnostic and therapeutic medicine.[8,9] Although lanthanides have no endogenous biological function in humans,[10] their trivalent ions can act as Ca^{2+} ion mimics by virtue of their similar ionic radii.[11] As such, the Ln ions may be useful for the treatment of bone resorption disorders,[12] where they behave as surrogates for Ca^{2+} in the hydroxyapatite-like matrix of bone.[13,14] Notably, the largest lanthanide, lanthanum, was efficiently incorporated into bone in preclinical studies,

Special Issue: Celebrating the Year of the Periodic Table: Emerging Investigators in Inorganic Chemistry

Received: May 1, 2019

DOI: 10.1021/acs.inorgchem.9b01277
Inorg. Chem. XXXX, XXX, XXX–XXX

Table 1. Clinically Relevant Radioisotopes of f-Block Elements and Their Properties

isotope	decay mode(s)	half-life (days)	application	clinical status	ref
^{134}La	β^+	4.48×10^{-3}	therapy/imaging		
^{135}La	EC[a]	0.79	therapy		52
^{134}Ce	EC	3.16	therapy		41
^{149}Pm	β^-	2.21	therapy	preclinical	44, 46
^{153}Sm	β^-	1.95	therapy	approved (1997)	46, 48
^{149}Tb	α/β^+	0.17	therapy/imaging	preclinical	42, 43, 46, 62, 63
^{152}Tb	β^+	0.73	imaging	preclinical	42, 46
^{155}Tb	EC	5.32	imaging	preclinical	42, 46
^{161}Tb	β^-	6.88	therapy	preclinical	42, 44, 46, 51
^{166}Ho	β^-	1.12	therapy	phase I/II	44–46
^{170}Tm	β^-	128.63	therapy	preclinical	46, 47
^{177}Lu	β^-	6.65	therapy	approved (2018)	44, 46, 49
^{225}Ac	α	9.92	therapy	phase I	64–68, 77, 78, 80–82
^{227}Th	α	18.69	therapy	phase I	68–76, 79
^{230}U	α	20.83	therapy		84, 85
^{252}Cf	SF[b]	0.97×10^3	therapy	phase II	89–91
^{255}Fm	α	0.84	therapy		86–88

[a]EC, electron capture. [b]SF, spontaneous fission.

demonstrating the potential use of this ion in diseases such as osteoporosis.[15−17] Furthermore, La^{3+} is a key component of the drug Fosrenol [$La_2(CO_3)_3$] for the treatment of hyperphosphatemia, a serious condition that is caused by elevated levels of phosphate in the blood. Administered as a simple carbonate salt, La^{3+} treats hyperphosphatemia by forming an insoluble phosphate salt that is cleared through the gastrointestinal tract, preventing its absorption into the body.[18] The FDA approval of this drug in 2004 highlights how a fundamental property of the lanthanides, namely, their poor aqueous solubility upon complexing phosphate, can be exploited in medicine.

Similarly, the unique magnetic and spectroscopic properties of lanthanides have made them indispensable in the field of imaging.[19] The most well-known Ln ion in medicine, Gd^{3+}, is used extensively in magnetic resonance imaging contrast agents; notably, all eight of the T_1-based contrast agents currently approved for use in the United States contain Gd^{3+} as the metal center.[20−22] Owing to the $S = {}^7/_2$ ground state of this ion afforded by its seven unpaired 4f electrons, Gd^{3+} enhances T_1 or the longitudinal relaxation rate of the ^{1}H nuclei of water surrounding tissues of interest, enabling high-resolution imaging of internal body structures such as cancerous lesions. Additionally, the lanthanides possess narrow emission energies, long luminescence lifetimes, and large Stokes shifts that arise from Laporte forbidden f−f electronic transitions.[23−28] Researchers have taken advantage of these unique photophysical properties to develop luminescent lanthanide-based imaging agents for subcellular structure,[29−31] bone integrity,[32−34] and tumor morphology.[35,36]

Lanthanides also possess a number of radioisotopes that are suitable for diagnostic and therapeutic applications in nuclear medicine (Table 1).[37−40] For diagnosis, radioisotopes that emit β^+ particles, or positrons, can be leveraged for use in positron emission tomography (PET) imaging. The emitted positrons rapidly annihilate with electrons in the surrounding tissue to release two γ photons that can be detected by imaging cameras. Single-photon emission tomography (SPECT) imaging can be carried out using radioisotopes that emit a single γ photon. Radiolanthanides that have been explored as imaging agents for PET or SPECT include ^{149}Tb, ^{152}Tb, ^{155}Tb, and ^{134}La.[41−43]

The therapeutic applications of f-block ions can be achieved by using radioisotopes that emit β particles, α particles, or Auger electrons. β particles have the same mass and charge as electrons and are ejected with high energy (0.5−2.3 MeV) from a decaying nucleus. A consequence of their high energy and low mass is a relatively high biological penetration range of these particles of up to 12 mm, which makes them useful for treating large solid tumors.[37] β-particle-emitting isotopes ^{177}Lu, ^{149}Pm, ^{153}Sm, ^{161}Tb, and ^{166}Ho have shown promise for the treatment of solid tumors in a wide range of cancers, with several drug candidates reaching clinical trials.[42,44−46] Preclinical studies involving the β emitter ^{170}Tm have demonstrated that ^{170}Tm-ethylenediaminetetramethylene phosphonic acid (^{170}Tm-EDTMP) is a cost-effective alternative to $^{89}SrCl_2$ for bone pain palliation associated with bone metastases.[47] The clinical utility of the β-emitting radiolanthanides has been further validated by the FDA approval of ^{153}Sm-lexidronam (Quadramet) in 1997 and ^{177}Lu-dotatate (Lutathera) in 2018 for the treatment of pain associated with bone metastases[48] and gastroenteropancreatic neuroendocrine tumors,[49] respectively.

The emission of Auger electrons occurs after radioactive decay by either electron capture or internal conversion. These decay modes generate vacancies in the 1s, 2s, and 2p core atomic orbitals. The relaxation of these high-energy core hole states occurs when an electron in a higher-energy orbital transitions downward to an orbital of lower energy, ejecting another electron in the process. These electron cascades release cytotoxic amounts of highly localized radiation that can cause significant damage to DNA in the cell nucleus.[50] By virtue of their low energy, Auger electrons have a very small biological penetration range that can be harnessed for precise intracellular targeting. Within the Ln series, ^{134}La, ^{135}La, ^{134}Ce, and ^{161}Tb have been identified as potential Auger emitters for therapeutic use.[41,51,52] At this point, however, there are no preclinical studies describing the full cytotoxic efficacy of these radionuclides.

DOI: 10.1021/acs.inorgchem.9b01277
Inorg. Chem. XXXX, XXX, XXX−XXX

Chart 1. Structures of the Ligands Discussed in This Work

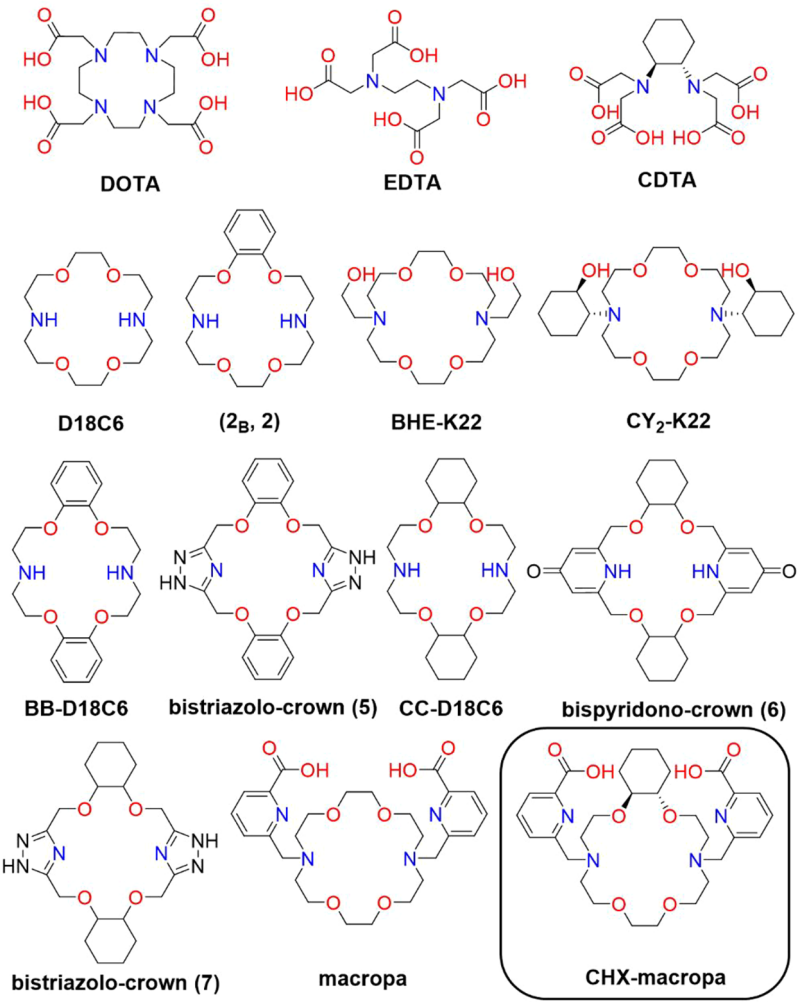

α-Particle-emitting radionuclides have garnered significant interest for their use in targeted α therapy (TAT)[53−55] based on several advantages that they possess over conventional β emitters.[56−58] Compared to the high penetration range of β particles, the significantly more massive α particles can only travel up to 100 μm in tissue. Despite this short range, α particles possess a high linear energy transfer and are quite effective at inducing cell death through DNA double-strand breaks.[59−61] These properties make α-emitting isotopes favorable for the treatment of small tumors for which there is high risk for nonspecific irradiation of nearby healthy tissue. Within the Ln series, ^{149}Tb is currently the only radionuclide that has been evaluated as an α emitter for clinical use.[42,43,62,63]

Actinides in Medicine. Moving further down the Periodic Table, the radioactive actinides (An) are most commonly considered in the context of nuclear energy or weapons. However, their radioactivity can also be harnessed for nuclear medicine (Table 1). More specifically, the α-emitting radionuclides ^{225}Ac[64−67] and ^{227}Th[68−76] are currently under intense investigation for use in TAT. In conjunction with different biological targeting vectors, these An radionuclides have progressed to clinical trials for the treatment of a range of cancers, including metastatic castration-resistant prostate cancer,[77−79] acute myeloid leukemia,[80,81] neuroendocrine tumors,[82] and tumors expressing mesothelin.[83] Additionally, a radioisotope of uranium, ^{230}U, has been identified as a promising candidate for TAT based, in part, on its relatively short half-life of 20.83 days.[84,85] Because the most stable form of uranium in oxygenated aqueous solution is the linear UO_2^{2+} ion, the implementation of ^{230}U in medicine will require the development of specifically tailored chelating agents.

Lastly, there may also be applications in medicine for the late synthetic actinides. For example, fermium, a man-made element that was first discovered in the debris of the detonation of the first hydrogen bomb,[86,87] has a radioisotope, ^{255}Fm, with suitable properties for use in TAT.[88] Although no serious efforts have been undertaken yet to evaluate this radionuclide for its therapeutic properties, it does highlight the intriguing possibility of using these exotic man-made elements to benefit society in the biomedical realm. Another transplutonium element that may have therapeutic value is californium. Specifically, ^{252}Cf, a radioisotope that was also discovered in the debris from the first thermonuclear test,[87] has been investigated for the treatment of a range of cancer types. ^{252}Cf undergoes decay by spontaneous fission (3.1% probability), rendering this radionuclide a strong source of neutrons that can be leveraged for brachytherapy, or internal radiation therapy.[89] It is anticipated that the promising clinical efficacy of ^{252}Cf demonstrated to date[90,91] will spark future research efforts directed toward the more widespread implementation of this synthetic actinide in medicine.

DOI: 10.1021/acs.inorgchem.9b01277
Inorg. Chem. XXXX, XXX, XXX−XXX

Scheme 1. Synthesis of CHX-macropa

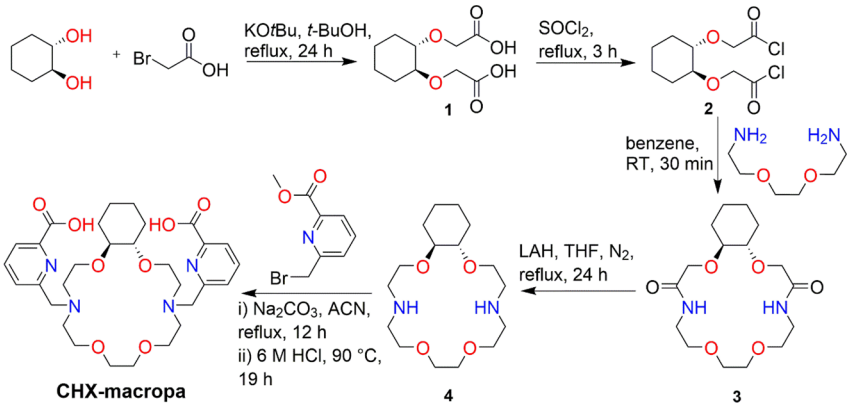

Ligand Design for f-Block Metals. To leverage the distinct properties of the 4f and 5f metal ions for medical applications, they need to be administered in a chelated form in vivo. Under most circumstances, chelators for these ions will be conjugated to a biological targeting vector, such as an antibody or peptide, that can deliver them to the desired locations in vivo. For these types of constructs to be effective, the chelating agents need to be appropriately matched to the ion of interest.[92] Generally, these ligands must possess two key features to be suitable for in vivo applications. First, the chelator should rapidly complex the metal center under mild conditions of pH and temperature. Fast metal-binding kinetics is particularly essential for applications that employ short-lived radioactive f-block ions, which can undergo considerable decay during the preparation of the radiopharmaceutical agent. The ability to chelate under mild conditions is also beneficial because the biological targeting vectors that are often used will decompose under conditions of extreme pH and temperature. A second requirement for these chelators is that they form complexes of high stability. Stable chelation in vivo is imperative because it will prevent the redistribution of these nonendogenous metal ions throughout the patient and the resulting toxicity from this off-target localization.

A key challenge in designing chelating agents for the biological use of the f-block elements resides in the general lability of these ions that results from the electrostatic nature of their bonding interactions. In particular, effective chelation strategies for large f-block metal ions such as La^{3+} and Ac^{3+} are scarce owing to their low charge density, which gives rise to longer and weaker metal−donor bonds that serve to destabilize the resulting complexes.[66] As such, the "normal" trend observed for the thermodynamic stability of f-block complexes is one that is inversely related to the ionic radius, where smaller ions form more stable ionic bonds with chelators than their larger counterparts. Thus, few options are available for the chelation of large lanthanides and actinides, a limitation that has hindered their implementation in medicine. The most widely used chelator for binding large 4f and 5f ions is the tetraazamacrocycle 1,4,7,10-tetraazacyclododecane-1,4,7,10-tetraacetic acid (DOTA; Chart 1). Although DOTA can adequately chelate the majority of trivalent lanthanides and actinides of medical interest, the stability of its complexes decreases significantly for larger ions,[93−96] like most conventional ligands. Given the lack of well-defined systems for the chelation of large f-block metal ions, there exists a critical need for new ligands with high affinity for large metals in order to capitalize on the valuable properties of these ions in medicine.

Tuning Size-Selectivity Patterns. In ongoing efforts to develop ligands that form stable complexes with large metal ions, we have investigated the coordination properties of macrocycles based on the 1,7,10,16-tetraoxa-4,13-diazacyclooctadecane (D18C6) core.[97,98] This 18-membered macrocycle (Chart 1) gives rise to ligands that exhibit an unusual thermodynamic preference for large over small metal ions.[99−108] As discussed above, this trend is in contrast to the majority of conventional poly(aminocarboxylate) ligands that form more stable complexes with smaller ions. Notably, our studies have revealed that macropa (Chart 1), a D18C6-based macrocycle possessing two picolinate pendent arms, can rapidly form a stable complex with $^{225}Ac^{3+}$, the largest 3+ ion in the Periodic Table.[97] Leveraging the therapeutic properties of this α-particle-emitting radionuclide (Table 1), we recently reported that a single dose of ^{225}Ac-RPS-074, an ^{225}Ac−macropa bifunctional construct that targets prostate cancer, induces complete tumor ablation in mice.[109] In addition to macropa's remarkable Ac-chelating properties, we and others have demonstrated its ability to selectively bind large Ln,[110] alkaline earth,[98,111] and p-block[111] metal ions over their smaller congeners. The unusual reverse-size selectivity of macropa fills an important niche in medicine, where bifunctional chelators for large metal ions are greatly needed.

On the basis of the success of macropa for chelating large metal ions of biomedical relevance, we sought to explore how further structural modifications of this ligand could alter or improve its reverse-size selectivity. In this Forum Article, we describe these efforts with a report on the synthesis and Ln-chelating properties of the novel ligand CHX-macropa, an analogue of macropa in which the ethylene bridge connecting two oxygen donors in the D18C6 backbone is replaced with a rigid cyclohexylene bridge. Our detailed thermodynamic evaluation of CHX-macropa with the Ln series reveals that complexes of this ligand are progressively destabilized relative to complexes of macropa as the ionic radius of the Ln ion decreases. Consequently, CHX-macropa is substantially more selective than macropa for large lanthanides. The underpinnings of this size-dependent destabilization were probed by density functional theory (DFT). Collectively, our studies show that the conformational rigidity in the D18C6 backbone can significantly influence f-block ion-selectivity patterns and be applied for the development of novel expanded macrocycles for use in medicine.

DOI: 10.1021/acs.inorgchem.9b01277
Inorg. Chem. XXXX, XXX, XXX−XXX

RESULTS AND DISCUSSION

Synthesis and Characterization of CHX-macropa. The synthesis of the decadentate macrocycle CHX-macropa was accomplished in six steps (Scheme 1). *trans*-1,2-Cyclohexanediyldioxydiacetic acid (**1**) was prepared from the alkylation of *trans*-1,2-cyclohexanediol with bromoacetic acid and then converted to the corresponding acyl chloride (**2**) according to established literature procedures.[112,113] Cyclization of **2** with commercially available 2,2′-(ethylenedioxy)bis(ethylamine) in benzene gave the diamide macrocycle **3** in good yield. Subsequent reduction of the amide groups using lithium aluminum hydride (LAH) in tetrahydrofuran (THF) afforded the novel *trans*-cyclohexyl-D18C6 macrocyclic scaffold (**4**). Picolinate groups were appended to the secondary amine nitrogen atoms of the macrocycle via alkylation with 6-(bromomethyl)pyridine-2-carboxylic acid methyl ester in acetonitrile (ACN) at reflux. Following hydrolysis of the methyl ester groups in 6 M HCl at 90 °C and purification of the product by semipreparative high-performance liquid chromatography (HPLC), CHX-macropa was isolated as a crystalline hydrochloride salt and characterized by ^{1}H and ^{13}C NMR spectroscopy, mass spectrometry, analytical HPLC, and elemental analysis (Figures S1−S11, in the Supporting Information, SI).

Single crystals of CHX-macropa suitable for X-ray diffraction were grown by vapor diffusion of diethyl ether into a methanol solution of the ligand. CHX-macropa crystallizes in the centrosymmetric $P2_1/c$ space group, which requires that both enantiomers of this ligand be present. This result is consistent with the use of racemic *trans*-1,2-cyclohexanediol as a starting reagent for the synthesis of the ligand. The asymmetric unit, shown in Figure 1, comprises the ligand dication and two chloride counteranions. The picolinic acid pendent arms of CHX-macropa are situated on opposite sides with respect to the plane of the cyclohexyl-D18C6 ring, which adopts a slightly puckered conformation. The cyclohexyl group of the macrocycle backbone achieves the chair conformation, the most stable configuration for cyclohexane. Each chloride anion engages in a hydrogen-bonding interaction with a protonated nitrogen atom of the macrocyclic ring, as well as with the carboxylic acid group of the corresponding picolinate arm attached to the nitrogen atom. Crystallographic parameters and interatomic distances and angles for [H_2CHX-macropa]Cl_2 are provided in Tables S1−S3.

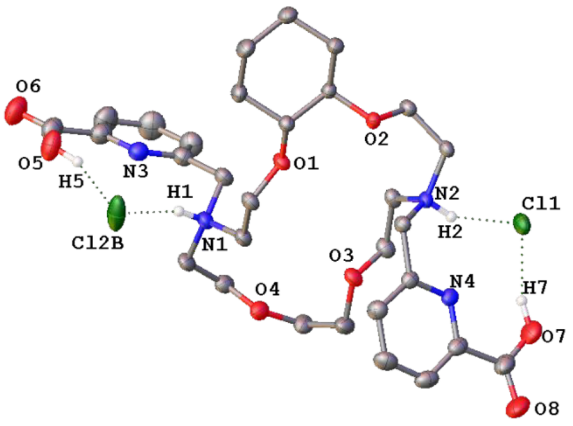

Figure 1. X-ray crystal structure of [H_2CHX-macropa]Cl_2. Hydrogen atoms attached to carbon centers are omitted for clarity. Thermal ellipsoids are drawn at the 50% probability level. One chloride counteranion (Cl2) is disordered over two positions and is shown at the highest occupied position (occupancy = 0.82). Dotted lines represent hydrogen-bonding interactions.

Thermodynamic Stability Studies. Increasing the conformational rigidity of a ligand can have a marked effect on its affinity for metal ions, giving rise to complexes of greater thermodynamic stability compared to complexes of the parent ligand.[114,115] A classic example of the successful implementation of this principle is the acyclic chelator *trans*-(1,2-diaminocyclohexane)tetraacetic acid (CDTA), an analogue of ethylenediaminetetraacetic acid (EDTA), where the ethylenediamine component is replaced with a rigid *trans*-diaminocyclohexane bridge (Chart 1). The stability constants of complexes of CDTA with most metal ions, including the lanthanides and actinides, are 1−5 orders of magnitude higher than those of EDTA.[116,117] This enhanced complex stability is attributed to the preorganization conferred by the cyclohexyl group, which locks the nitrogen atoms of the ligand in the *gauche* conformation that is required for metal chelation. Accordingly, the thermodynamics of complex formation are more favorable for CDTA than for EDTA, which has to undergo a configurational rearrangement to attain the correct geometry for metal binding.[118]

Despite many examples in the literature of constrained macrocycles,[119,120] few efforts to date have been directed at decreasing the conformational mobility of ligands containing the D18C6 scaffold to modulate metal-binding affinity. Notably, the ligands (2_B, 2),[121] in which one benzene ring is fused into the D18C6 backbone, and CY_2-K22,[122] which has two rigid 2-hydroxycyclohexyl arms appended to D18C6, exhibit increased affinity for small metal ions and decreased affinity for large metal ions compared to their respective nonrigid parent ligands D18C6 and BHE-K22 (Chart 1). Because of this divergence in affinity, both conformationally constrained ligands have augmented size selectivity for small metal ions. Other rigidified D18C6 ligands have been synthesized (Chart 1), but their coordination chemistry has not been evaluated in detail.[112,123−125] These limited studies underscore the need for further exploration of the effects of conformational flexibility on the size selectivity of this class of macrocycles.

To systematically probe the thermodynamic consequences of reinforcing the bridge of one chelate ring of macropa's D18C6 scaffold with a fused cyclohexyl group, we determined the protonation constants of CHX-macropa and the stability constants of its metal complexes with the entire Ln series (except Pm) using pH potentiometry. The results are compiled in Table 2. The protonation constants and Ln stability constants previously reported for macropa are provided for comparison.[110] From the titration of CHX-macropa in the absence of metal ions, four protonation constants (log K_{ai}; eq 1) were determined over a pH range of 2.3−11. These values correspond to the sequential protonation of the two amine nitrogen atoms of the macrocycle (log K_{a1} and log K_{a2}) and the two pyridinecarboxylate pendent groups (log K_{a3} and log K_{a4}). The fifth and sixth ligand protonation constants are out of the range of measurement for our potentiometric system (log K_a < 2) and therefore could not be determined. A comparison of the ligand protonation constants reveals that the macrocyclic nitrogen atoms of CHX-macropa are slightly more basic relative to macropa; the first protonation constant is increased by 0.36 log K units, and the second protonation constant is

DOI: 10.1021/acs.inorgchem.9b01277
Inorg. Chem. XXXX, XXX, XXX−XXX

Table 2. Protonation Constants of CHX-macropa and Macropa[a] and Thermodynamic Stability Constants of Their Ln^{3+} Complexes Determined by pH Potentiometry (25 °C and I = 0.1 M KCl)

	CHX-macropa^{2-}	macropa^{2-} [b]
log K_{a1}	7.77(1)[c]	7.41
log K_{a2}	6.95(1)	6.85
log K_{a3}	3.17(4)	3.32
log K_{a4}	2.51(7)	2.36
log K_{a5}		1.69
log K_{LaL}	14.54(1)	14.99
log K_{LaHL}		2.28
log K_{CeL}	14.38(3)	15.11
log K_{CeHL}		2.07
log K_{PrL}	13.89(1)	14.70
log K_{PrHL}		2.96
log K_{NdL}	13.57(5)	14.36
log K_{NdHL}		2.08
log K_{SmL}	12.79(1)	13.80
log K_{SmHL}		2.70
log K_{EuL}	12.25(3)	13.01
log K_{EuHL}		1.97
log K_{GdL}	11.53(2)	13.02
log K_{GdHL}		2.48
log K_{TbL}	10.98(4)	11.79
log K_{TbHL}		2.91
log K_{DyL}	10.34(3)	11.72
log K_{DyHL}		2.42
log K_{HoL}	9.67(5)	10.59
log K_{ErL}	8.96(6)	10.10
log K_{TmL}	8.19(3)	9.59
log K_{YbL}	7.44(4)	8.89
log K_{LuL}	6.70(1)	8.25

[a]Data provided for comparison. [b]Reference 110. [c]The standard deviation is given in parentheses and corresponds to the last digit of the stability constant.

increased by 0.1 log K units. The overall basicities[126] of the two ligands, however, are very similar, with the sum of their log K_a values equaling 20.4 for CHX-macropa and 21.6 for macropa.

$$K_{ai} = \frac{[H_iL]}{[H_{i-1}L][H^+]} \quad (1)$$

$$K_{ML} = \frac{[ML]}{[M][L]} \quad (2)$$

$$K_{MH_iL} = \frac{[MH_iL]}{[MH_{i-1}L][H^+]} \quad (3)$$

Stability constants, or log K_{ML} values (eq 2), for complex formation were measured from potentiometric titrations of CHX-macropa carried out in the presence of equimolar Ln^{3+} ions (Table 2 and Figure S12). For the smaller lanthanides Tb−Lu, monoprotonated complexes (MHL) could not be reasonably modeled based on the titration data over the pH range investigated. For the larger lanthanides Ce−Gd, log K_{MHL} values (eq 3) ranging from 1.23 to 2.23 could be refined in the model, but these values carried a high standard deviation in most cases. We attribute this to the fact that only a minor amount of monoprotonated species (<10%) would be present in solution across the pH range investigated, thereby preventing the accurate determination of log K_{MHL}. Removing the MHL species from the model did not significantly change the values of log K_{ML}. Therefore, in contrast to macropa, log K_{MHL} values have not been reported for CHX-macropa because of our uncertainties regarding the significance of this equilibrium.

In comparison to macropa, the stability constants of the lanthanide complexes of CHX-macropa are consistently lower across this series. Despite this general reduction of the affinity for the lanthanides, CHX-macropa retains selectivity for large over small lanthanides, with stability constants for the large lanthanides approaching those of macropa (Table 2 and Figure 2a). For example, the log K_{ML} value of 14.54 measured for La−CHX-macropa is similar to that of 14.99 for La−macropa. Although the stability constants of macropa and CHX-macropa are comparable for the early lanthanides, these values become more disparate for the mid and late lanthanides, which possess increasingly smaller ionic radii (Figure 2a). Notably, the stability constant of the complex of CHX-macropa with Lu^{3+}, the smallest lanthanide ion, is 1.55 log K units lower than that of Lu−macropa. A plot of Δlog K_{ML}, the difference in the stability constants between macropa and CHX-macropa, versus the ionic radii of the lanthanides highlights the differences between the size selectivity of these ligands (Figure 2b). Specifically, this plot reveals that complexes of CHX-macropa are increasingly destabilized relative to their macropa analogues as the ionic radius of the Ln ion decreases, a trend that is reflected by an increase in the absolute value of Δlog K_{ML} upon moving across the Ln series. The poorer affinity of CHX-macropa for the small lanthanides renders this ligand 10 times more selective than macropa for La^{3+} over Lu^{3+} (log K_{LaL} − log K_{LuL} = 7.84 for CHX-macropa and 6.74 for macropa). Thus, the integration of a rigid cyclohexyl group into the D18C6 scaffold of macropa leads to a significant enhancement in the reverse-size selectivity for large lanthanides.

X-ray Structure of La−CHX-macropa. To assess the impact of the cyclohexyl bridge in CHX-macropa on the structural architecture of its metal complexes, the solid-state structure of the La^{3+} complex of CHX-macropa was obtained using single-crystal X-ray diffraction. The complex was formed in situ by mixing equimolar amounts of the ligand and $LaCl_3 \cdot 6.8H_2O$ in water (~37 mM) and adjusting the pH to 7 with dilute potassium hydroxide (KOH). Potassium hexafluorophosphate (KPF_6, ~7.5 equiv) was added to the solution, and single crystals suitable for X-ray diffraction were isolated from slow evaporation of the solution. The complex crystallized in the $P2_1/c$ space group with one PF_6^- counteranion and two water molecules in the outer sphere, giving a formula of $[La(CHX\text{-}macropa)(OH_2)]PF_6 \cdot 2H_2O$. Although the initial refinement of the crystal structure proceeded as expected, a large residual electron density remained near the La center. Further analysis of these data revealed that the origin of this residual density could be explained by whole-molecule disorder. This whole-molecule disorder was refined, as described in detail in the Supporting Information (see section 5 and Figures S13 and S14), to give two components of the $[La(CHX\text{-}macropa)(OH_2)]^+$ cation with occupancies of 0.85 and 0.15. Both components of the whole-molecule disorder were identical with respect to coordination geometries and ligand conformation. As such, our discussion here is based on the major occupancy component. Crystallographic parameters and interatomic distances and angles for both components are given in Tables S1, S4, and S5.

DOI: 10.1021/acs.inorgchem.9b01277
Inorg. Chem. XXXX, XXX, XXX−XXX

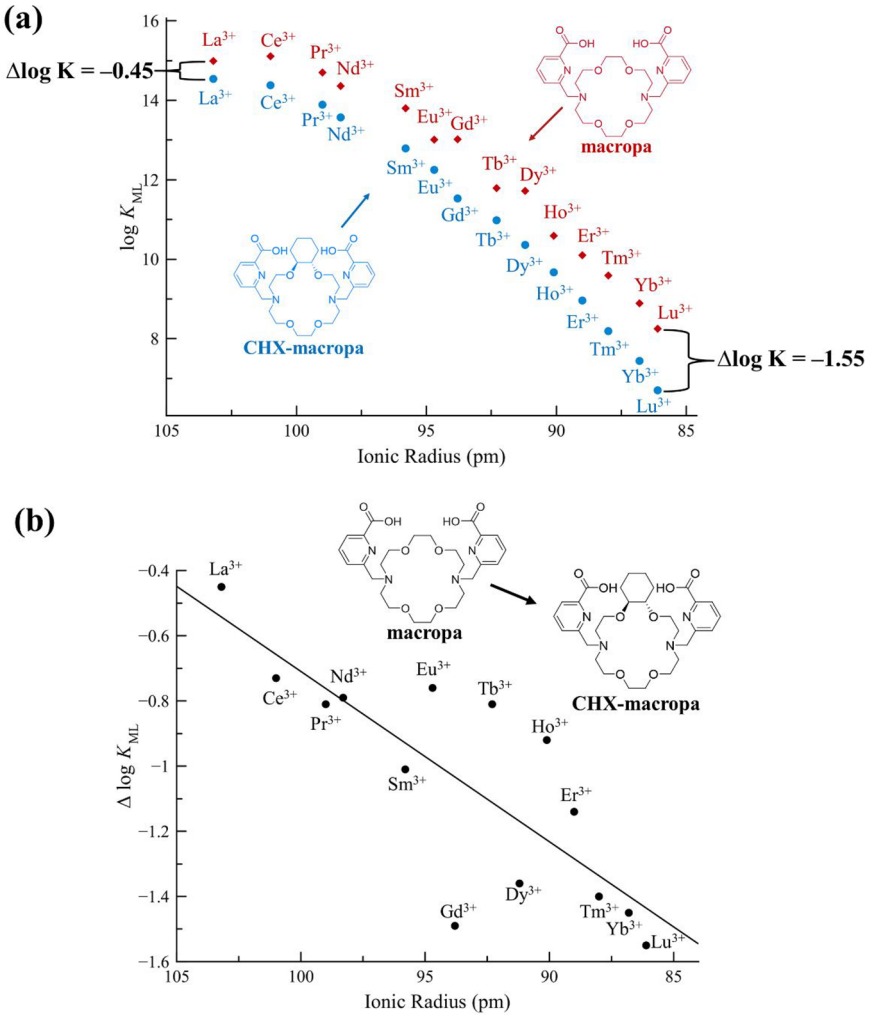

Figure 2. Effects of substituting an ethylene bridge in macropa's D18C6 core with a cyclohexylene bridge in CHX-macropa on the thermodynamic complex stability and size selectivity, plotted as a function of the 6-coordinate ionic radius of each Ln^{3+} ion. (a) Comparison between the Ln stability constants (log K_{ML} values) of CHX-macropa (blue circles) and macropa (red diamonds). (b) Plot of the change in the complex stability, Δlog K_{ML}, in passing from macropa to CHX-macropa. Δlog K = log $K_{Ln-CHX\text{-}macropa}$ − log $K_{Ln-macropa}$.

The crystal structure reveals that all 10 atoms of the N_4O_6 donor set are coordinated to the La^{3+} center, with the picolinate pendent arms positioned on the same side of the macrocycle in a *syn* conformation (Figure 3). A water molecule, penetrating from underneath the macrocycle, completes the undecadentate coordination sphere. The positions of the hydrogen atoms of the water molecules (inner and outer sphere) could not be definitively located on the difference Fourier map, most likely because of the whole-molecule disorder. Their presence, however, is inferred based on close contacts within the crystal lattice that reflect hydrogen-bonding interactions. The absolute configuration of the ligand can be assigned using Δ or Λ symbols to denote the helical twist of the picolinate pendent arms and δ or λ to designate the chirality of each of the six 5-membered chelate rings.[127] The conformations of the La−CHX-macropa complex in the crystal structure are $\Delta(\delta\lambda\delta)(\delta\lambda\delta)$ and its enantiomer $\Lambda(\lambda\delta\lambda)(\lambda\delta\lambda)$. As expected, the *trans*-cyclohexyl group is positioned in the chair configuration, which is required for the oxygen atoms of the macrocycle to attain the correct orientation for metal binding. Notably, the structural arrangement of $[La(CHX\text{-}macropa)(OH_2)]^+$ is consistent with that reported previously[97] for $[La(Hmacropa)(OH_2)]^{2+}$ and other complexes of macropa with large metal ions.[98,111] This similarity suggests that the incorporation of a cyclohexyl group in the ligand backbone does not significantly perturb the overall conformation of the La^{3+} complex.

Although the whole-molecule disorder of $[La(CHX\text{-}macropa)(OH_2)]^+$ prevents a detailed discussion of the interatomic distances within this complex, some general observations can be made. The La1A−N1A and La1A−N2 distances in the structure of $[La(CHX\text{-}macropa)(OH_2)]^+$ are 2.943 and 2.878 Å, respectively. The similarity of these values reflects the fact that the metal center is situated centrally within the macrocycle. However, the interatomic distances between La1A and the ether donor atoms of the macrocycle, O1A, O2A, O3A, and O4A, vary more significantly, ranging from 2.779 to 2.988 Å. Notably, both the shortest and longest La−O interatomic distances reside on the side of the D18C6 ring bearing the cyclohexyl group. For comparison, the crystal structure of $[La(macropa)(OH_2)]^+$ shows that all four of the $La-O_{ether}$ interatomic distances are within 0.1 Å of each other. The disparate La−O interatomic distances in $[La(CHX\text{-}macropa)(OH_2)]^+$ are corroborated by DFT calculations below and may be a consequence of the rigidity of the

DOI: 10.1021/acs.inorgchem.9b01277
Inorg. Chem. XXXX, XXX, XXX−XXX

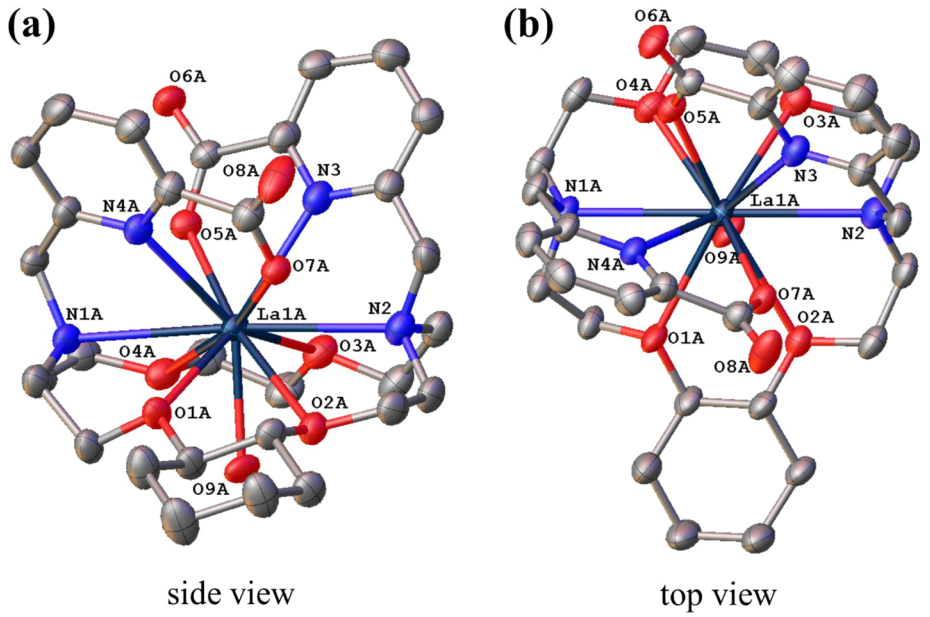

Figure 3. X-ray crystal structure of $[La(CHX\text{-}macropa)(OH_2)]PF_6 \cdot 2H_2O$ viewed from the (a) side and (b) top. Hydrogen atoms attached to carbon centers, the PF_6^- counteranion, and outer-sphere water molecules are omitted for clarity. Thermal ellipsoids are drawn at the 50% probability level. Owing to a whole-molecule disorder (see the main text), the positions of the hydrogen atoms of the coordinated water molecule could not be assigned. Only the major component (occupancy = 0.85) is shown.

cyclohexylene group that prevents all of the donor atoms of the macrocycle from optimally interacting with the metal center.

DFT Calculations. The thermodynamic studies described above indicate that the addition of a cyclohexyl group into a ligand scaffold can confer enhanced reverse-size selectivity to CHX-macropa by disfavoring the formation of stable complexes with small metal ions. Similar results were reported for related macrocyclic ligands in which adjacent nitrogen donors were bridged to form piperazine rings.[128,129] For these previously reported ligands, the decreased stability of complexes of smaller metal ions was attributed to the conformational rigidity of the ligands, which inhibited their abilities to attain geometries suitable for small ion binding. To probe the role of the conformational rigidity on the Ln-binding properties of CHX-macropa, DFT calculations were carried out at the TPSSh/LC RECP/6-31G(d,p) level of theory. We selected the TPSSh functional and large-core relativistic effective core potential (LC RECP) approach based on previous studies that have demonstrated this functional and core potential to yield more accurate results for Ln complexes in comparison to other common functionals.[130,131] Coordinates for the optimized structures are included in the SI. To verify the accuracy of our computational approach, we first calculated the aqueous Gibbs free energy (ΔG_{aq}) for the exchange reaction shown in eq 4:

$$[La(L)]^+(aq) + Ln^{3+}(aq) \xrightarrow{\Delta G_{aq}} [Ln(L)]^{3+}(aq) + La^{3+}(aq) \quad (4)$$

This calculation was achieved through the use of the thermodynamic cycle[131−134] presented in Scheme 2, where ΔG_g is the Gibbs free energy of the gas-phase reaction and ΔG_{sol} is the solvation free energy for the complex in water.

For the Ln^{3+} ions, previously optimized polarizable continuum model (PCM) radii were used in all solvation calculations.[131,135] No scaling factor was applied to these radii

Scheme 2. Thermodynamic Cycle Showing the Relationship between ΔG_g and ΔG_{aq}

$$\begin{array}{ccccc} [La(L)]^+_{(g)} & + & Ln^{3+}_{(g)} & \xrightarrow{\Delta G_g} & [Ln(L)]^+_{(g)} + La^{3+}_{(g)} \\ \downarrow \Delta G_{sol}([La(L)]^+) & & \downarrow \Delta G_{sol}(Ln^{3+}) & & \downarrow \Delta G_{sol}([Ln(L)]^+) \quad \downarrow \Delta G_{sol}(La^{3+}) \\ [La(L)]^+_{(aq)} & + & Ln^{3+}_{(aq)} & \xrightarrow{\Delta G_{aq}} & [Ln(L)]^+_{(aq)} + La^{3+}_{(aq)} \end{array}$$

in subsequent computations (α = 1.0). Using this approach, ΔG_{aq} can be calculated from eq 5:

$$\Delta G_{aq} = \Delta G_g + \Delta G_{sol}([Ln(L)]^+) + \Delta G_{sol}(La^{3+}) - \Delta G_{sol}(Ln^{3+}) - \Delta G_{sol}([La(L)]^+) \quad (5)$$

The calculated ΔG_{aq} values for both ligands (Figure S15 and Table S6) are in very good agreement with the experimental data and previous DFT-calculated values for macropa,[131] verifying the accuracy of this computational approach.

To investigate the origin of the enhanced size selectivity of CHX-macropa compared to macropa, we first considered the conformational preference of the ligands. A previous analysis of the stability of Ln−macropa complexes demonstrated a rather abrupt change in the conformational preference of the ligand as the lanthanide series was traversed.[110] For the larger lanthanides, the $\Delta(\delta\lambda\delta)(\delta\lambda\delta)$ conformation was observed to be the most energetically stable, whereas the smaller lanthanides were most stable with the $\Delta(\lambda\delta\lambda)(\lambda\delta\lambda)$ conformation. To determine if the Ln complexes of CHX-macropa had a similar trend in conformational preferences, we computationally determined the relative energies of these conformations for the complexes of La^{3+}, Gd^{3+}, and Lu^{3+}. The relative energies of eight different ligand conformations, calculated with the solvation model based on density (SMD) implicit solvation model for water, are reported in Figure 4.

DOI: 10.1021/acs.inorgchem.9b01277
Inorg. Chem. XXXX, XXX, XXX−XXX

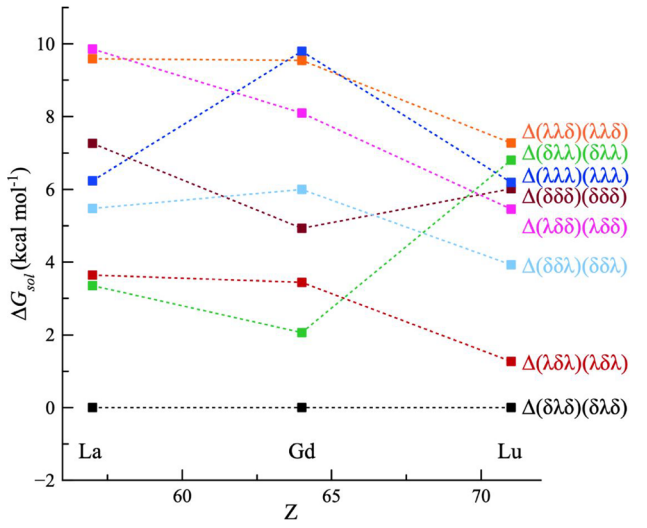

Figure 4. Relative SMD free energies (ΔG_{sol}) of the eight conformations of $[Ln(CHX\text{-}macropa)]^+$ complexes (Ln = La, Gd, Lu) in aqueous solution. Energies are reported relative to the $\Delta(\delta\lambda\delta)(\delta\lambda\delta)$ conformation.

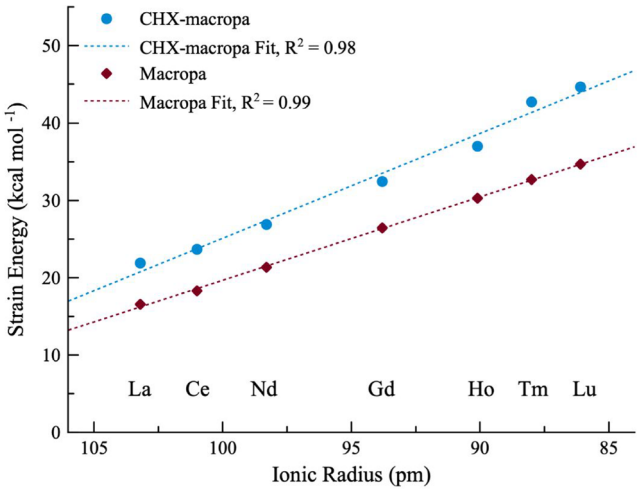

Figure 5. Calculated strain energies for macropa (red diamonds) and CHX-macropa (blue circles) as a function of the ionic radius. Values are reported relative to the energy of the optimized free ligand, which was normalized to zero. Dashed lines represent the linear fit of the data. The ionic radii of the Ln ions are reported based on a coordination number of 6.

These calculations reveal that, for CHX-macropa, the $\Delta(\delta\lambda\delta)$-$(\delta\lambda\delta)$ conformation is the lowest-energy conformation for all of the lanthanides evaluated. For La^{3+}, the $\Delta(\delta\lambda\delta)(\delta\lambda\delta)$ conformation is calculated to be 3.35 kcal mol^{-1} lower in energy than the next-lowest-energy conformation $\Delta(\delta\lambda\lambda)$-$(\delta\lambda\lambda)$. This preference is consistent with the crystal structure of $[La(CHX\text{-}macropa)(OH_2)]^+$, which attains this $\Delta(\delta\lambda\delta)$-$(\delta\lambda\delta)$ conformation. Similarly, the Lu^{3+} complex of CHX-macropa is calculated to be most stable in the $\Delta(\delta\lambda\delta)(\delta\lambda\delta)$ conformation. The $\Delta(\lambda\delta\lambda)(\lambda\delta\lambda)$ conformation is only marginally higher in energy (1.27 kcal mol^{-1}). By contrast, the Lu^{3+} complex of macropa energetically favors the $\Delta(\lambda\delta\lambda)(\lambda\delta\lambda)$ conformation over the $\Delta(\delta\lambda\delta)(\delta\lambda\delta)$ conformation by 6.1 kcal mol^{-1}.[110] Thus, macropa has strong conformational preferences in a manner that is dependent on the size of the Ln ion. CHX-macropa, on the other hand, maintains a thermodynamic preference for a single conformation across the entire Ln series regardless of the ionic radii. We hypothesize that this effect arises from the enhanced rigidity of the diazacrown backbone provided by the cyclohexyl functionality, which restricts its conformational freedom and prevents the ligand from attaining an optimal configuration for interacting with the small Ln ions. Thus, this effect may contribute to the enhanced reverse size selectivity of CHX-macropa.

The energy required for a ligand to distort from its relaxed equilibrium conformation to bind a metal ion is its strain energy. The magnitude of this strain energy can have a pronounced effect on the metal-ion size selectivity of polydentate ligands.[93,115,136] To determine the role of the strain energy in the Ln ion selectivity of CHX-macropa, this energy was computed via DFT for several representative Ln-ion complexes of macropa and CHX-macropa.[137] The strain energies for both chelators increase linearly ($R^2 \geqslant 0.98$) with decreasing ionic radius of the Ln ion (Figure 5). The strain energies of CHX-macropa are consistently larger than those for macropa, which is most likely a consequence of the greater rigidity of the cyclohexyl backbone. The slopes of these linear regressions, however, are different. The values of these slopes are −1.36 and −1.08 kcal mol^{-1} pm^{-1} for CHX-macropa and macropa, respectively. The larger magnitude of the slope in the linear regression for CHX-macropa indicates that the strain energy of this ligand is more sensitive to ionic radius changes than macropa. This result highlights the influence of the increased conformational rigidity of CHX-macropa on the steric strain and size selectivity within this class of ligands.

The coordination geometry of metal complexes of macrocycles can also reveal structural features that may reflect their relative stabilities. For example, complexes of macropa with large metals such as Sr^{2+}, Pb^{2+}, La^{3+}, and Ba^{2+} hold these ions centrally in the macrocycle; interatomic distances between chemically equivalent donor atoms and metal centers are all nearly equal.[97,98,111] By contrast, thermodynamically less stable complexes of smaller metal ions such as Lu^{3+} exhibit a somewhat asymmetric coordination environment; interatomic distances between the donor atoms and metal centers are disparate.[97] Thus, there appears to be a correlation between the thermodynamic stability and structural features of these complexes. Analysis of the DFT-optimized structures may therefore provide additional insight on the stabilities of these complexes. The DFT-optimized structure of $[Lu(macropa)]^+$ captures the incongruous Lu−O_C (O_C = crown ether oxygen) distances observed experimentally, which span values ranging from 2.596 to 2.8 Å. For $[La(macropa)]^+$, the La−O_C distances are all nearly equivalent, suggesting that macropa can optimally bind the large La^{3+} ion but not the small Lu^{3+} ion.[97] Analysis of the $[Ln(CHX\text{-}macropa)]^+$ DFT-optimized structures reveals that the metal coordination environment becomes increasingly disparate as the f block is traversed from large to small lanthanides (Figure S16). In comparison to $[Lu(macropa)]^+$ (max−min: Lu−N_{AM} = 0 Å; Lu−O_C = 0.208 Å), the calculated range of metal−donor distances is greater for $[Lu(CHX\text{-}macropa]^+$ (max−min: Lu−N_{AM} = 0.143 Å; Lu−O_C = 0.218 Å). For both $[La(macropa)]^+$ and $[La(CHX\text{-}macropa)]^+$, however, these distances are nearly equivalent. This analysis of the geometric parameters shows that the donor atom interactions of CHX-macropa with small metal ions are less effective than those of macropa.

Kinetic Inertness of Complexes. The kinetic inertness of metal complexes is of utmost importance when using f-block

DOI: 10.1021/acs.inorgchem.9b01277
Inorg. Chem. XXXX, XXX, XXX−XXX

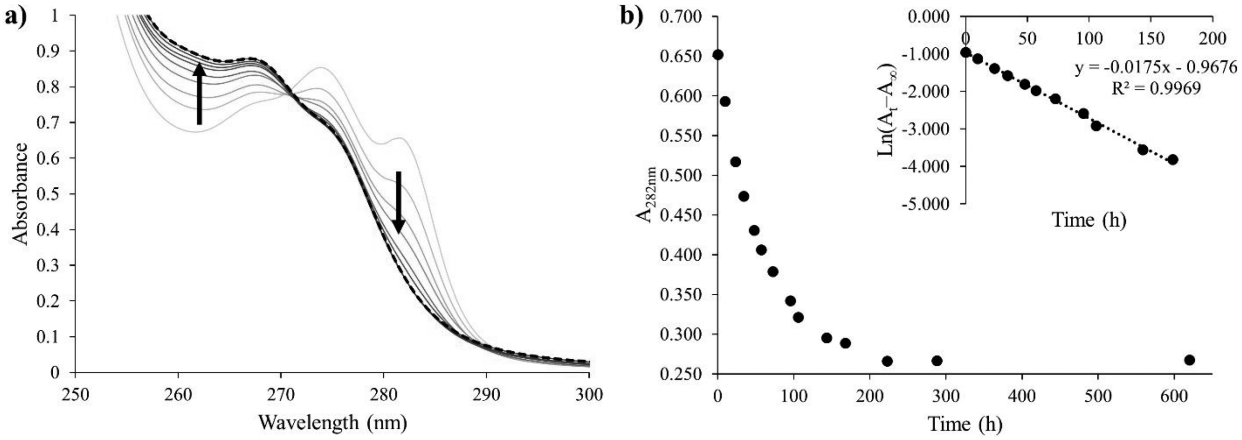

Figure 6. Stability of La−CHX-macropa in the presence of a competing ligand. (a) Time course of the UV spectra of La−CHX-macropa in pH 7.4 MOPS buffer at room temperature with 1000 equiv of DTPA. The final spectrum matches that of a solution of CHX-macropa with 1000 equiv of DTPA (black dotted line), confirming that no intact La−CHX-macropa complex remains. (b) Plot of the change in absorbance at 282 nm versus time. Inset: Linear fit of the data to the first-order integrated rate law.

ions in medicine. Free metal ions released from metallodrugs in vivo accumulate in various tissues of the body, such as the bone, giving rise to toxic side effects that can prevent their clinical use in therapeutic and diagnostic applications. Although the affinity of macropa for La^{3+} (log K_{LaL} = 14.99)[110] is 4.5 orders of magnitude lower than that of diethylenetriaminepentaacetic acid (DTPA; log K_{LaL} = 19.48),[138] we previously observed that La−macropa is stable for up to 21 days when challenged with a 1000-fold excess of DTPA.[97] This remarkable inertness of La−macropa, despite its lower thermodynamic stability, underscores the fact that kinetic stability cannot be predicted on the basis of thermodynamic affinity.

On the basis of this rationale, we investigated the stability of La^{3+}, Gd^{3+}, and Lu^{3+} complexes of CHX-macropa against transchelation by DTPA using UV−vis spectrophotometry. Challenges were performed at room temperature in pH 7.4 3-(*N*-morpholino)propanesulfonic acid (MOPS) buffer (100 mM) by adding excess DTPA to the complexes formed in situ. For comparison, these challenges were also carried out with macropa. The transchelation of the complexes was monitored using changes with time of the $\pi-\pi^*$ absorption at 282 and 285 nm. Under the pseudo-first-order conditions employed, La−CHX-macropa exhibited moderate kinetic stability when challenged with 1000 equiv of DTPA, undergoing transchelation with a half-life of 39 ± 1 h (Figure 6). By contrast, La−macropa was approximately 87% intact after 23 days (Figure S17). The stability of La−macropa is reduced slightly from our previous study, in which we used 10 mM instead of 100 mM MOPS.[97] Therefore, there may be a small effect of the buffer composition on the rate of transchelation. Gd−CHX-macropa displayed 10-fold reduced kinetic stability compared to Gd−macropa, corresponding to half-lives of 52 ± 1 and 555 ± 11 s, respectively, in the presence of 1000 equiv of DTPA (Figures S18 and S19). For complexes of both CHX-macropa and macropa with Lu^{3+}, the amount of DTPA employed in the study was reduced to only 10 equiv. Nonetheless, the kinetics of transchelation was so rapid that half-lives could not be determined (<20 s; Figures S20 and S21). Collectively, these results indicate that the increased rigidification of CHX-macropa leads to an increase in the kinetic lability of its Ln complexes in comparison to macropa. This result is somewhat unexpected based on the successful enhancement of kinetic stability afforded by other cyclohexyl-rigidified chelators.[139−142] Thus, these studies highlight that more subtle kinetic effects may be operational during the decomplexation of metal ions.

CONCLUSIONS

Although the f-block elements reside at the bottom of the Periodic Table in a region that is largely neglected by many pharmaceutical scientists, these ions have important applications in the realm of medicine, as highlighted in this Forum Article. A key requirement for their biological use is the development of appropriate chelating agents that can stably retain and deliver them in vivo. In this work, we have described our efforts to optimize the large f-block ion chelator macropa by installing a rigid cyclohexyl group on the macrocycle backbone. Our results have shown that rigidification of the macrocycle was generally ineffective for increasing both the thermodynamic and kinetic stabilities of Ln complexes. These results contrast with previous studies that have shown that ligand rigidification using the cyclohexyl group is a highly effective strategy for developing more stable complexes, indicating that additional factors may be operational. Despite the poorer stabilities of Ln complexes of CHX-macropa, this ligand exhibited an enhanced thermodynamic selectivity for large lanthanides over small lanthanides, a property that was supported by DFT calculations to be a consequence of its increased structural rigidity. Therefore, we have shown that rigidifying the diaza-18-crown-6 scaffold of macropa with the cyclohexylene group is a promising strategy to tune the ion size selectivity of this class of ligands. Although CHX-macropa may not be directly useful for f-element chelation in the biomedical realm, it may be a valuable ligand for the separation of large lanthanides from small lanthanides. Ongoing efforts are directed toward exploring the potential of CHX-macropa for this application.

EXPERIMENTAL SECTION

Synthesis. All solvents and reagents, unless otherwise noted, were of ACS grade or higher and were purchased from commercial sources. Solvents noted as dry were obtained following storage over 3 Å molecular sieves. $[N(CH_3)_4][OH]$ was purchased as a 25 wt % solution in water (H_2O; trace metals basis, Beantown Chemical, Hudson, NH). Concentrated hydrochloric acid (HCl; BDH Aristar

DOI: 10.1021/acs.inorgchem.9b01277
Inorg. Chem. XXXX, XXX, XXX−XXX

Plus, VWR, Radnor, PA) and metal salts (various commercial suppliers) were of trace metal grade. Deionized H_2O (≥18 MΩ cm) was obtained from an Elga Purelab Flex 2 water purification system.

High-performance liquid chromatography (HPLC) consisted of a CBM-20A communications bus module, an LC-20AP (preparative) or LC-20AT (analytical) pump, and an SPD-20AV UV−vis detector monitoring at 270 nm (Shimadzu, Japan). Analytical chromatography was carried out using an Ultra Aqueous C18 column, 100 Å, 5 μm, 250 mm × 4.6 mm (Restek, Bellefonte, PA) at a flow rate of 1.0 mL min^{-1}. Semipreparative purification was performed using an Epic Polar preparative column, 120 Å, 10 μm, 25 cm × 20 mm (ES Industries, West Berlin, NJ) at a flow rate of 14 mL min^{-1}. NMR spectra were recorded at 25 °C on a Varian Inova 600 MHz spectrometer or on a Bruker AV III HD 500 MHz spectrometer equipped with a broadband Prodigy cryoprobe. Chemical shifts are reported in parts per million. Spectra acquired in $CDCl_3$ were referenced to a tetramethylsilane internal standard (0 ppm). Samples prepared in D_2O were spiked with ACN, and the spectra were referenced to the corresponding signal at either 2.06 ppm (^1H) or 1.47 ppm (^{13}C). The splitting of proton resonances in the reported ^1H NMR spectra is defined as s = singlet, d = doublet, t = triplet, m = multiplet, and br = broad. High-resolution mass spectra were obtained on an Exactive Orbitrap mass spectrometer in positive-ion electrospray ionization (ESI) mode (ThermoFisher Scientific, Waltham, MA). UV−vis spectra were recorded on a Cary 8454 UV−vis spectrometer (Agilent Technologies, Santa Clara, CA) using 1 cm quartz cuvettes. Elemental analysis was performed by Atlantic Microlab, Inc. (Norcross, GA).

Macropa ($2HCl{\cdot}3.5H_2O$) was synthesized according to a literature procedure,[110,143] except 6-(bromomethyl)pyridine-2-carboxylic acid methyl ester[144] was used instead of 6-(chloromethyl)pyridine-2-carboxylic acid methyl ester. *trans*-1,2-Cyclohexanediyldioxydiacetic acid (**1**)[112] and *trans*-1,2-cyclohexanediyldioxydicetyl dichloride (**2**)[113] were prepared according to literature procedures, except bromoacetic acid was used in place of chloroacetic acid for the synthesis of **1**. Purification of **1** by recrystallization from ethyl acetate, as previously reported,[112] was unsuccessful. Instead, the crude residue of this compound was purified by silica gel column chromatography using dichloromethane (DCM) as the eluent. Fractions were pooled and concentrated to give an amber oil, from which a white solid precipitated upon standing overnight. The solid was filtered, washed with DCM, and dried in vacuo, furnishing **1** in 7% yield.

*rac-(16aS,20aS)/(16aR,20aR)-Dodecahydro-2H,11H-benzo[b]-[1,4,10,13]tetraoxa[7,16]diazacyclooctadecine-3,14(4H,15H)-dione (**3**).* The synthesis of **3** was adapted from a general procedure for the preparation of similar macrocycles.[145] Compound **2** (1.54 g, 5.7 mmol) in benzene (39 mL) and 2,2′-(ethylenedioxy)bis(ethylamine) (1.58 mL, 10.8 mmol) in benzene (39 mL) were simultaneously added dropwise over approximately 10 min to a flask containing vigorously stirring benzene (95 mL) at room temperature. The resulting pale-yellow suspension was stirred for an additional 30 min and then filtered. The flask and filtered solid were rinsed with benzene (3 × 20 mL), and the faintly yellow filtrate was concentrated under reduced pressure to an off-white solid. Column chromatography [silica gel, 0−2.5% methanol (MeOH) in $CHCl_3$] afforded the title compound as a white solid (1.34 g, 68% yield). ^1H NMR (500 MHz, $CDCl_3$): δ 7.68 (br t, 2H), 4.18−3.99 (m, 4H), 3.70−3.63 (m, 2H), 3.62−3.47 (m, 8H), 3.46−3.35 (m, 2H), 3.31−3.20 (m, 2H), 2.21−2.06 (m, 2H), 1.83−1.66 (m, 2H), 1.25−1.07 (m, 4H). $^{13}C\{^1H\}$ NMR (126 MHz, $CDCl_3$): δ 170.50, 81.83, 70.01, 69.38, 67.59, 39.25, 29.59, 23.87. ESI-MS. Found: *m/z* 711.37820. Calcd for $[C_{32}H_{56}N_4O_{12}Na]^+$: *m/z* 711.37869. Found: *m/z* 367.18373. Calcd for $[C_{16}H_{28}N_2O_6Na]^+$: *m/z* 367.18396. Found: *m/z* 345.20185. Calcd for $[C_{16}H_{29}N_2O_6]^+$: *m/z* 345.20201.

*rac-(16aS,20aS)/(16aR,20aR)-Hexadecahydro-2H,11H-benzo[b]-[1,4,10,13]tetraoxa[7,16]diazacyclooctadecine (**4**).* The synthesis of **4** was adapted from a general procedure for the reduction of similar macrocyclic diamides.[145] A three-necked round-bottom flask under a positive atmosphere of N_2 was charged with lithium aluminum hydride (LAH; 1.03 g, 27.1 mmol) and dry tetrahydrofuran (THF, 26 mL). A hot suspension of **3** (1.31 g, 3.8 mmol) in dry THF (11 mL) was slowly added to the chilled suspension of LAH, and the gray mixture was heated at reflux for 24 h. The reaction mixture was subsequently cooled in an ice bath, and the excess LAH was destroyed by the careful addition of 50:50 H_2O/THF (∼8 mL). The mixture was vacuum filtered on sintered glass equipped with a nylon membrane (0.22 μm), and the filtered solid was washed with 3 portions of hot benzene (100 mL total). The filtrate was concentrated under reduced pressure to an oil, which was redissolved in DCM (∼25 mL), dried over sodium sulfate, and concentrated to give macrocycle **4** as a pale-yellow oil (1.00 g, 83% yield). ^1H NMR (600 MHz, $CDCl_3$): δ 3.79−3.70 (m, 2H), 3.66−3.56 (m, 10H), 3.21−3.14 (m, 2H), 2.90−2.73 (m, 8H), 2.11−2.03 (m, 2H), 1.71−1.62 (m, 2H), 1.21−1.10 (m, 4H). $^{13}C\{^1H\}$ NMR (126 MHz, $CDCl_3$): δ 81.71, 70.00, 69.66, 67.75, 49.57, 49.20, 30.37, 24.14. ESI-MS. Found: *m/z* 317.24279. Calcd for $[C_{16}H_{33}N_2O_4]^+$: *m/z* 317.24348. Found: *m/z* 159.12507. Calcd for $[C_{16}H_{34}N_2O_4]^{2+}$: *m/z* 159.12538.

rac-6,6′-[[(16aS,20aS)/(16aR,20aR)-Hexadecahydro-4H,13H-benzo[b][1,4,10,13]tetraoxa[7,16]diazacyclooctadecine-4,13-diyl]-bis(methylene)]dipicolinic acid (CHX-macropa). 6-(Bromomethyl)-pyridine-2-carboxylic acid methyl ester[144] (0.740 g, 3.2 mmol) and Na_2CO_3 (1.06 g, 10.0 mmol) were added to a slight suspension of **4** in dry ACN (33 mL). The resulting mixture was heated at reflux and stirred overnight. It was then concentrated under reduced pressure, and the pale-yellow residue was dissolved in DCM (30 mL) and washed with H_2O (15 mL). The organic layer was separated, and the aqueous layer was extracted two more times with DCM (30 mL). The combined organics were backextracted with H_2O (5 mL), dried over sodium sulfate, and concentrated under reduced pressure to give a cloudy orange-yellow oil. ESI-MS. Found: *m/z* 637.32460. Calcd for $[C_{32}H_{46}N_4O_8Na]^+$: *m/z* 637.32079. Found: *m/z* 615.34266. Calcd for $[C_{32}H_{47}N_4O_8]^+$: *m/z* 615.33884. Found: *m/z* 308.17495. Calcd for $[C_{32}H_{48}N_4O_8]^{2+}$: *m/z* 308.17306.

The oil was redissolved in 6 M HCl (4 mL) and heated at 90 °C for 15 h. The orange-brown reaction solution was then concentrated on a rotary evaporator, and the crude residue was purified by reverse-phase semipreparative HPLC using a binary mobile phase containing 0.1% CF_3COOH (program: 10% MeOH/H_2O for 5 min, followed by a linear gradient to 100% MeOH over 35 min). Pure fractions were combined and concentrated under reduced pressure. To prepare the hydrochloride salt, the residue was dissolved repeatedly in 6 M HCl and concentrated on a rotary evaporator, and then dried in vacuo for 48 h to give the title compound as a off-white, crystalline solid (0.494 g, 42% yield). ^1H NMR (500 MHz, D_2O, pD ≈ 1−2): δ 8.17 (d, *J* = 7.8 Hz, 2H), 8.10 (t, *J* = 7.8 Hz, 2H), 7.74 (d, *J* = 7.7 Hz, 2H), 4.77−4.67 (m, 4H), 4.04−3.84 (m, 8H), 3.73−3.50 (m, 12H), 3.33−3.22 (m, 2H), 1.99−1.88 (m, 2H), 1.60−1.48 (m, 2H), 1.13−1.00 (m, 2H), 0.98−0.81 (m, 2H). $^{13}C\{^1H\}$ NMR (126 MHz, D_2O, pD ≈ 1−2): δ 168.05, 150.43, 147.56, 140.71, 128.74, 126.25, 82.37, 70.28, 64.73, 62.36, 58.48, 55.25, 55.18, 29.58, 23.57. ESI-MS. Found: *m/z* 587.31030. Calcd for $[C_{30}H_{43}N_4O_8]^+$: *m/z* 587.30754. Found: *m/z* 294.15875. Calcd for $[C_{30}H_{44}N_4O_8]^{2+}$: *m/z* 294.15741. Elem anal. Found: C, 49.16; H, 6.56; N, 7.47. Calcd for $C_{30}H_{42}N_4O_8{\cdot}3.2HCl{\cdot}1.8H_2O$: C, 48.97; H, 6.69; N, 7.61. HPLC: t_R = 18.70 min.

X-ray Diffraction Measurements. Low-temperature X-ray diffraction data for crystals of $[H_2CHX\text{-macropa}]Cl_2$ and $[La(CHX\text{-macropa})(OH_2)]PF_6{\cdot}2H_2O$ were collected on a Rigaku XtaLAB Synergy diffractometer coupled to a Rigaku Hypix detector with Cu Kα radiation (λ = 1.54184 Å) from a PhotonJet microfocus X-ray source at 100 K. The diffraction images were processed and scaled using the *CrysAlisPro* software (2015, Rigaku OD, The Woodlands, TX). The structures were solved through intrinsic phasing using *SHELXT*[146] and refined against F^2 on all data by full-matrix least squares with *SHELXL*[147] following established refinement strategies.[148] All non-hydrogen atoms were refined anisotropically. All hydrogen atoms bound to carbon atoms were included in the model at geometrically calculated positions and refined using a riding model. Hydrogen atoms bound to oxygen and nitrogen atoms were located in the difference Fourier map, if possible, and subsequently refined semifreely with the help of distance restraints. The isotropic

DOI: 10.1021/acs.inorgchem.9b01277
Inorg. Chem. XXXX, XXX, XXX−XXX

displacement parameters of all hydrogen atoms were fixed to 1.2 times the U_{eq} value of the atoms that they are linked to (1.5 times for methyl groups). In the structure of $[H_2CHX\text{-macropa}]Cl_2$, one chloride counterion was disordered over two positions, which was modeled using the *PART* command, with the occupancies summing to 1 (Cl2A 0.18; Cl2B 0.82). The structure of $[H_2CHX\text{-macropa}]Cl_2$ contains one heavily disordered methanol molecule, which is located on a crystallographic center of inversion and has been modeled using the solvent mask routine in *Olex*^{2} (volume, 246.8 Å^3; e$^-$ count, 32).[149] The rationale and procedure for the structure refinement of $[La(CHX\text{-macropa})(OH_2)]PF_6{\cdot}2H_2O$, which exhibited whole-molecule disorder, are detailed in the SI. Our approach to addressing this crystallographic problem in a systematic manner followed procedures outlined for a previously reported osmium(VI) nitrido complex that also crystallized with whole-molecule disorder.[150] Crystallographic data collection and refinement parameters, interatomic distances, and interatomic angles are given in Tables S1−S5.

Solution Thermodynamics. Potentiometric titrations were carried out using a Metrohm Titrando 888 titrator equipped with a Ross Orion combination electrode (8103BN, ThermoFisher Scientific), a Metrohm 806 exchange unit with an automatic buret (10 mL), and *Tiamo 2.5* software. The titration vessel was fitted with a removable glass cell (∼70 mL) and thermostated at 25 °C using a Thermomix 1442D circulating H_2O bath. CO_2 was excluded from the vessel using a small positive pressure of argon scrubbed with 30 wt % KOH. Carbonate-free KOH (∼0.1 M) was prepared by the dissolution of pellets (semiconductor grade, 99.99% trace metals basis, Sigma-Aldrich) or by the dilution of Baker Dilut-It analytical concentrate (Avantor) using freshly boiled H_2O (⩾18 MΩ cm) and standardized by potentiometric titration against potassium hydrogen phthalate. HCl (0.1 M, J.T. Baker) was standardized against Tris base (J.T. Baker). All titration solutions were maintained at a constant ionic strength of 0.1 M using KCl (BioUltra, ⩾99.5%, Sigma-Aldrich) and equilibrated for 25 min prior to the addition of titrant.

Before every ligand or ligand−metal titration, the electrode was calibrated in terms of the hydrogen-ion concentration by titrating a solution of standardized HCl (5 mM) containing a supporting electrolyte (H/KCl = 0.1 M) with standardized KOH. Data within the pH ranges of 2.3−3.2 and 10.8−11.2 were analyzed using the program *Glee* (version 3.0.21)[151] to obtain the standard electrode potential (E_0) and slope factor. The H_2O ion product (pK_w = 13.78) was taken from the literature.[152] Prior to titrations containing La^{3+} and Ce^{3+} metal ions, which form complexes of high stability with CHX-macropa, the electrode was calibrated to pH 2.0 by using a higher concentration of HCl (10 mM).

$LnCl_3$ salts were dissolved in 0.1 M HCl to give stock solutions of the metal ions. The concentrations of these solutions were determined by complexometric titration in a NaOAc buffer (100 mM, pH 5.5) with a standardized solution of ethylenediaminetetraacetic acid disodium salt (Alfa Aesar, 57.5 mM). Xylenol orange (1 mg mL^{-1}, 4 drops) was used as the indicator. A stock solution of CHX-macropa was prepared in H_2O, and its exact concentration was calculated in triplicate from the volume difference between the two sharp end points of its potentiometric titration curve with KOH.

The ligand protonation constants and stability constants of Ln^{3+} complexes were measured by adding standardized KOH to an aqueous solution (20 mL) containing ligand (∼0.022 mmol), 0.1 M HCl (0.1 mmol), and 1 M KCl (1.9 mmol) in the absence and presence of metal ion (∼0.022 mmol), respectively. The titration method employed a 0.1 mV min^{-1} drift limit and a maximum wait time of 180 s (protonation constants) or 300 s (stability constants) between the addition of aliquots of base. For metal−ligand titrations, a minimum wait time of 120 s was also enforced. If the drift criterion was not satisfied within the maximum wait time, the point was excluded from the titration data set. Additionally, data beyond the end point (pH ∼7) in metal−ligand titrations were omitted owing to precipitation of $Ln(OH)_3$ at high pH. Back titrations with 0.1 M HCl were performed once for each Ln−ligand combination to verify that equilibrium was attained at each data point under the given conditions. Only the back titration of CHX-macropa with La^{3+} displayed poor reversibility. A titration in which the minimum wait time between the addition of aliquots of base was increased to 10 min gave rise to the same calculated stability constant as when the minimum wait time was 120 s, indicating that the hysteresis between forward and back titrations arises from slow complex dissociation rather than formation kinetics.

The protonation and stability constants were refined using the program *Hyperquad2013*.[153] Only the proton concentration was admitted as a refineable parameter. The protonation constants, defined in eq 1, were calculated from the average of seven titrations using data points from pH 2.3 to 11. With the protonation constants in hand, the stepwise stability constants (eq 2) and protonation constants of the metal complexes (eq 3) were calculated from the average of three forward titrations. Hydrolysis constants for the formation of $Ln(OH)^{2+}$ in aqueous solution were included in the model.[154] The errors provided correspond to 1 standard deviation.

Computational Methods. DFT calculations were performed using the *Gaussian09* software,[155] following procedures similar to those previously described.[131,134,156] Macropa[97] and CHX-macropa were optimized in the deprotonated state starting from their respective crystal structures. The starting geometries for the metal complexes were taken from previous computational studies on macropa.[110] Inner-sphere H_2O molecules were not included in the optimization of the metal complexes. Geometries of the complexes were optimized in the gas phase at 298 K using the TPSSh functional.[157] Light atoms (hydrogen, carbon, nitrogen, and oxygen) were treated with the 6-31G(d,p) basis set, and metal atoms were assigned the LC RECP and related (7s6p5d)/[5s4p3d] basis set.[158,159] The LC RECP calculations include 46 + 4f^n electrons in the core of the metal center, leaving the outermost 5s, 5p, 5d, and 6s electrons to be handled explicitly. As such, all calculations were performed in the pseudosinglet state. This method has been previously justified by the corelike properties of the f electrons.[131,160−162] Frequency calculations were performed to confirm that the calculated structures were local minima on the potential energy surface and to determine the thermodynamic properties of the complexes. Solvation energies were calculated using the SMD method, and thermodynamic parameters in H_2O were estimated by taking the thermodynamic corrections from gas-phase calculations as previously described.[163] Hydration free energies of the Ln^{3+} ions were calculated as previously described using the SMD solvation model and parametrized PCM radii.[131,135] Basis set superposition errors, which arise from the use of finite basis sets and lead to an overestimation of the binding energy, were calculated in the gas phase using the Counterpoise method,[164,165] as implemented in *Gaussian09*, and these energies were included in the metal-exchange reaction calculations. Optimized coordinates for the complexes are given in the SI. The strain energy is reported as the difference in energy between the optimized structure of the free ligand and the single-point energy of the ligand in the geometry of the metal complex, with the metal ion removed at the TPSSh/6-31G(d,p) level of theory. All free ligand structures were handled in the deprotonated state.

Transchelation Challenges. The kinetic stabilities of complexes of La^{3+}, Gd^{3+}, and Lu^{3+} with CHX-macropa and macropa were evaluated in the presence of excess diethylenetriaminepentaacetic acid (DTPA) in a manner similar to that previously described.[97] All challenges were carried out in 100 mM pH 7.4 MOPS (I = 1 M with $[N(CH_3)_4][Cl]$, with the pH adjusted using aqueous $[N(CH_3)_4][OH]$). An aqueous solution of DTPA (125 mM) was prepared at pH 7.4 using $[N(CH_3)_4][OH]$ and diluted to 1.25 mM with MOPS buffer. Ln−L complexes were formed in situ by combining equimolar amounts (500 μM) of standardized $LnCl_3$ solution (0.1 M HCl) and ligand (H_2O) in MOPS buffer. Challenges were initiated by adding an aliquot of the Ln−L complex (500 μL) to a cuvette containing 125 or 1.25 mM DTPA (2000 μL). La−L and Gd−L complexes were challenged with 1000-fold excess DTPA (100 mM), and Lu−L complexes were challenged with 10-fold excess DTPA (1 mM). UV−vis spectra were acquired at various intervals (at least 10 data points) until there were no further spectral changes, except for samples containing La−macropa, which were monitored for 23 days. Pseudo-

DOI: 10.1021/acs.inorgchem.9b01277
Inorg. Chem. XXXX, XXX, XXX−XXX

first-order rate constants (k_{obs}) for transchelation of the complexes were calculated from the slopes of the plots of $\ln(A_t - A_\infty)$ versus time using linear regression. A_∞ is the final absorbance value, and A_t is the absorbance value at time t. Absorbance values were monitored at 282 nm for La^{3+} and 285 nm for Gd^{3+}. Half-lives ($t_{1/2}$) were calculated using the equation $t_{1/2} = \ln(2)/k_{obs}$ and are reported as the mean of three replicates ±1 standard deviation.

■ ASSOCIATED CONTENT

Supporting Information

The Supporting Information is available free of charge on the ACS Publications website at DOI: 10.1021/acs.inorgchem.9b01277.

Spectral characterization of synthesized compounds, details of computational and crystallographic studies, supporting figures for DFT and transchelation studies, and optimized coordinates from DFT calculations (PDF)

Accession Codes

CCDC 1913153 and 1913154 contain the supplementary crystallographic data for this paper. These data can be obtained free of charge via www.ccdc.cam.ac.uk/data_request/cif, or by emailing data_request@ccdc.cam.ac.uk, or by contacting The Cambridge Crystallographic Data Centre, 12 Union Road, Cambridge CB2 1EZ, UK; fax: +44 1223 336033.

■ AUTHOR INFORMATION

Corresponding Author

*E-mail: jjw275@cornell.edu.

ORCID

Nikki A. Thiele: 0000-0003-3301-0849

Joshua J. Woods: 0000-0002-6213-4093

Justin J. Wilson: 0000-0002-4086-7982

Author Contributions

[§]These authors contributed equally.

Notes

The authors declare no competing financial interest.

■ ACKNOWLEDGMENTS

J.J.W. is supported by the NSF-GRFP (Grant DGE-1650441). This work was supported by Cornell University. This research made use of the NMR Facility at Cornell University, which is supported, in part, by the NSF under Award CHE-1531632. A. S. Ivanov and V. S. Bryantsev (Chemical Sciences Division, Oak Ridge National Laboratory, Oak Ridge, TN) are thanked for their helpful correspondence involving DFT calculations.

■ REFERENCES

(1) Rosenberg, B.; VanCamp, L.; Krigas, T. Inhibition of Cell Division in *Escherichia coli* by Electrolysis Products from a Platinum Electrode. *Nature* **1965**, *205*, 698−699.

(2) Rosenberg, B.; VanCamp, L.; Trosko, J. E.; Mansour, V. H. Platinum Compounds: A New Class of Potent Antitumour Agents. *Nature* **1969**, *222*, 385−386.

(3) Rosenberg, B.; VanCamp, L. The Successful Regression of Large Solid Sarcoma 180 Tumors by Platinum Compounds. *Cancer Res.* **1970**, *30*, 1799−1802.

(4) Alderden, R. A.; Hall, M. D.; Hambley, T. W. The Discovery and Development of Cisplatin. *J. Chem. Educ.* **2006**, *83*, 728−734.

(5) Barry, N. P. E.; Sadler, P. J. Exploration of the Medical Periodic Table: Towards New Targets. *Chem. Commun.* **2013**, *49*, 5106−5131.

(6) Fricker, S. P. Metal Based Drugs: From Serendipity to Design. *Dalton Trans.* **2007**, 4903−4917.

(7) Mjos, K. D.; Orvig, C. Metallodrugs in Medicinal Inorganic Chemistry. *Chem. Rev.* **2014**, *114*, 4540−4563.

(8) Fricker, S. P. The Therapeutic Application of Lanthanides. *Chem. Soc. Rev.* **2006**, *35*, 524−533.

(9) Teo, R. D.; Termini, J.; Gray, H. B. Lanthanides: Applications in Cancer Diagnosis and Therapy. *J. Med. Chem.* **2016**, *59*, 6012−6024.

(10) Skovran, E.; Martinez-Gomez, N. C. Just Add Lanthanides. *Science* **2015**, *348*, 862−863.

(11) Evans, C. H. Interesting and Useful Biochemical Properties of Lanthanides. *Trends Biochem. Sci.* **1983**, *8*, 445−449.

(12) Weekes, D. M.; Orvig, C. Harnessing the Bone-Seeking Ability of Ca(II)-like Metal Ions in the Treatment of Metastatic Cancer and Resorption Disorders. *Chem. Soc. Rev.* **2016**, *45*, 2024−2031.

(13) Fernandez-Gavarron, F.; Huque, T.; Rabinowitz, J. L.; Brand, J. G. Incorporation of 140-Lanthanum into Bones, Teeth and Hydroxyapatite. *Bone Miner.* **1988**, *3*, 283−291.

(14) Cawthray, J. F.; Creagh, A. L.; Haynes, C. A.; Orvig, C. Ion Exchange in Hydroxyapatite with Lanthanides. *Inorg. Chem.* **2015**, *54*, 1440−1445.

(15) Barta, C. A.; Sachs-Barrable, K.; Jia, J.; Thompson, K. H.; Wasan, K. M.; Orvig, C. Lanthanide Containing Compounds for Therapeutic Care in Bone Resorption Disorders. *Dalton Trans.* **2007**, 5019−5030.

(16) Mawani, Y.; Cawthray, J. F.; Chang, S.; Sachs-Barrable, K.; Weekes, D. M.; Wasan, K. M.; Orvig, C. *In Vitro* Studies of Lanthanide Complexes for the Treatment of Osteoporosis. *Dalton Trans.* **2013**, *42*, 5999−6011.

(17) Cawthray, J. F.; Weekes, D. M.; Sivak, O.; Creagh, A. L.; Ibrahim, F.; Iafrate, M.; Haynes, C. A.; Wasan, K. M.; Orvig, C. *In Vivo* Study and Thermodynamic Investigation of Two Lanthanum Complexes, $La(dpp)_3$ and La(XT), for the Treatment of Bone Resorption Disorders. *Chem. Sci.* **2015**, *6*, 6439−6447.

(18) Albaaj, F.; Hutchison, A. J. Lanthanum Carbonate (Fosrenol®): A Novel Agent for the Treatment of Hyperphosphataemia in Renal Failure and Dialysis Patients. *Int. J. Clin. Pract.* **2005**, *59*, 1091−1096.

(19) Heffern, M. C.; Matosziuk, L. M.; Meade, T. J. Lanthanide Probes for Bioresponsive Imaging. *Chem. Rev.* **2014**, *114*, 4496−4539.

(20) Bottrill, M.; Kwok, L.; Long, N. J. Lanthanides in Magnetic Resonance Imaging. *Chem. Soc. Rev.* **2006**, *35*, 557−571.

(21) Major, J. L.; Meade, T. J. Bioresponsive, Cell-Penetrating, and Multimeric MR Contrast Agents. *Acc. Chem. Res.* **2009**, *42*, 893−903.

(22) Wahsner, J.; Gale, E. M.; Rodríguez-Rodríguez, A.; Caravan, P. Chemistry of MRI Contrast Agents: Current Challenges and New Frontiers. *Chem. Rev.* **2019**, *119*, 957−1057.

(23) Evans, C. H. *Biochemistry of the Lanthanides*; Springer: Boston, MA, 1990.

(24) Blasse, G.; Grabmaier, B. C. How Does a Luminescent Material Absorb Its Excitation Energy? In *Luminescent Materials*; Springer: Berlin, Heidelberg, 1994; pp 10−32.

(25) Kettle, S. F. A. f Electron Systems: The Lanthanides and Actinides. In *Physical Inorganic Chemistry: A Coordination Chemistry Approach*; Springer: Berlin, Heidelberg, 1996; pp 238−268.

(26) Moore, E. G.; Samuel, A. P. S.; Raymond, K. N. From Antenna to Assay: Lessons Learned in Lanthanide Luminescence. *Acc. Chem. Res.* **2009**, *42*, 542−552.

(27) Bünzli, J.-C. G. On the Design of Highly Luminescent Lanthanide Complexes. *Coord. Chem. Rev.* **2015**, *293*−*294*, 19−47.

(28) Sy, M.; Nonat, A.; Hildebrandt, N.; Charbonnière, L. J. Lanthanide-Based Luminescence Biolabelling. *Chem. Commun.* **2016**, *52*, 5080−5095.

(29) Cieslikiewicz-Bouet, M.; Eliseeva, S. V.; Aucagne, V.; Delmas, A. F.; Gillaizeau, I.; Petoud, S. Near-Infrared Emitting Lanthanide(III) Complexes as Prototypes of Optical Imaging Agents with Peptide Targeting Ability: A Methodological Approach. *RSC Adv.* **2019**, *9*, 1747−1751.

(30) Deiters, E.; Song, B.; Chauvin, A.-S.; Vandevyver, C. D. B.; Gumy, F.; Bünzli, J.-C. G. Luminescent Bimetallic Lanthanide

DOI: 10.1021/acs.inorgchem.9b01277
Inorg. Chem. XXXX, XXX, XXX−XXX

Bioprobes for Cellular Imaging with Excitation in the Visible-Light Range. *Chem. - Eur. J.* **2009**, *15*, 885−900.
(31) Walton, J. W.; Bourdolle, A.; Butler, S. J.; Soulie, M.; Delbianco, M.; McMahon, B. K.; Pal, R.; Puschmann, H.; Zwier, J. M.; Lamarque, L.; Maury, O.; Andraud, C.; Parker, D. Very Bright Europium Complexes That Stain Cellular Mitochondria. *Chem. Commun.* **2013**, *49*, 1600−1602.
(32) McMahon, B.; Mauer, P.; McCoy, C. P.; Lee, T. C.; Gunnlaugsson, T. Selective Imaging of Damaged Bone Structure (Microcracks) Using a Targeting Supramolecular Eu(III) Complex As a Lanthanide Luminescent Contrast Agent. *J. Am. Chem. Soc.* **2009**, *131*, 17542−17543.
(33) Vitha, T.; Kubíček, V.; Hermann, P.; Vander Elst, L.; Muller, R. N.; Kolar, Z. I.; Wolterbeek, H. T.; Breeman, W. A. P.; Lukeš, I.; Peters, J. A. Lanthanide(III) Complexes of Bis(Phosphonate) Monoamide Analogues of DOTA: Bone-Seeking Agents for Imaging and Therapy. *J. Med. Chem.* **2008**, *51*, 677−683.
(34) McMahon, B. K.; Mauer, P.; McCoy, C. P.; Lee, T. C.; Gunnlaugsson, T. Luminescent Terbium Contrast Agent for Bone Microdamage Detection. *Aust. J. Chem.* **2011**, *64*, 600−603.
(35) Li, Y.; Zeng, S.; Hao, J. Non-Invasive Optical Guided Tumor Metastasis/Vessel Imaging by Using Lanthanide Nanoprobe with Enhanced Down-Shifting Emission beyond 1500 nm. *ACS Nano* **2019**, *13*, 248−259.
(36) Xue, Z.; Zeng, S.; Hao, J. Non-Invasive through-Skull Brain Vascular Imaging and Small Tumor Diagnosis Based on NIR-II Emissive Lanthanide Nanoprobes beyond 1500 nm. *Biomaterials* **2018**, *171*, 153−163.
(37) Srivastava, S. C.; Mausner, L. F. Therapeutic Radionuclides: Production, Physical Characteristics, and Applications. In *Therapeutic Nuclear Medicine*; Baum, R., Ed.; Springer: Berlin, Heidelberg, 2013; pp 11−50.
(38) Amoroso, A. J.; Fallis, I. A.; Pope, S. J. A. Chelating Agents for Radiolanthanides: Applications to Imaging and Therapy. *Coord. Chem. Rev.* **2017**, *340*, 198−219.
(39) Van de Voorde, M.; Van Hecke, K.; Cardinaels, T.; Binnemans, K. Radiochemical Processing of Nuclear-Reactor-Produced Radiolanthanides for Medical Applications. *Coord. Chem. Rev.* **2019**, *382*, 103−125.
(40) Kostelnik, T. I.; Orvig, C. Radioactive Main Group and Rare Earth Metals for Imaging and Therapy. *Chem. Rev.* **2019**, *119*, 902−956.
(41) Lubberink, M.; Lundqvist, H.; Tolmachev, V. Production, PET Performance and Dosimetric Considerations of ^{134}Ce/^{134}La, an Auger Electron and Positron-Emitting Generator for Radionuclide Therapy. *Phys. Med. Biol.* **2002**, *47*, 615−629.
(42) Müller, C.; Zhernosekov, K.; Köster, U.; Johnston, K.; Dorrer, H.; Hohn, A.; van der Walt, N. T.; Türler, A.; Schibli, R. A Unique Matched Quadruplet of Terbium Radioisotopes for PET and SPECT and for α- and β-Radionuclide Therapy: An In Vivo Proof-of-Concept Study with a New Receptor-Targeted Folate Derivative. *J. Nucl. Med.* **2012**, *53*, 1951−1959.
(43) Müller, C.; Vermeulen, C.; Köster, U.; Johnston, K.; Türler, A.; Schibli, R.; van der Meulen, N. P. Alpha-PET with Terbium-149: Evidence and Perspectives for Radiotheragnostics. *EJNMMI Radiopharmacy and Chemistry* **2016**, *1*, 5.
(44) Uusijärv, H.; Bernhardt, P.; Rösch, F.; Maecke, H. R.; Forssell-Aronsson, E. Electron- and Positron-Emitting Radiolanthanides for Therapy: Aspects of Dosimetry and Production. *J. Nucl. Med.* **2006**, *47*, 807−814.
(45) Smits, M. L. J.; Nijsen, J. F. W.; van den Bosch, M. A. A. J.; Lam, M. G. E. H.; Vente, M. A. D.; Mali, W. P. T. M.; van Het Schip, A. D.; Zonnenberg, B. A. Holmium-166 Radioembolisation in Patients with Unresectable, Chemorefractory Liver Metastases (HEPAR Trial): A Phase 1, Dose-Escalation Study. *Lancet Oncol.* **2012**, *13*, 1025−1034.
(46) Mishiro, K.; Hanaoka, H.; Yamaguchi, A.; Ogawa, K. Radiotheranostics with Radiolanthanides: Design, Development Strategies, and Medical Applications. *Coord. Chem. Rev.* **2019**, *383*, 104−131.
(47) Das, T.; Chakraborty, S.; Sarma, H. D.; Tandon, P.; Banerjee, S.; Venkatesh, M.; Pillai, M. R. A. ^{170}Tm-EDTMP: A Potential Cost-Effective Alternative to $^{89}SrCl_2$ for Bone Pain Palliation. *Nucl. Med. Biol.* **2009**, *36*, 561−568.
(48) Kaitin, K. I.; Healy, E. M. The New Drug Approvals of 1996, 1997, and 1998: Drug Development Trends in the User Fee Era. *Drug Inf. J.* **2000**, *34*, 1−14.
(49) Strosberg, J.; El-Haddad, G.; Wolin, E.; Hendifar, A.; Yao, J.; Chasen, B.; Mittra, E.; Kunz, P. L.; Kulke, M. H.; Jacene, H.; Bushnell, D.; O'Dorisio, T. M.; Baum, R. P.; Kulkarni, H. R.; Caplin, M.; Lebtahi, R.; Hobday, T.; Delpassand, E.; Van Cutsem, E.; Benson, A.; Srirajaskanthan, R.; Pavel, M.; Mora, J.; Berlin, J.; Grande, E.; Reed, N.; Seregni, E.; Öberg, K.; Lopera Sierra, M.; Santoro, P.; Thevenet, T.; Erion, J. L.; Ruszniewski, P.; Kwekkeboom, D.; Krenning, E. Phase 3 Trial of ^{177}Lu-Dotatate for Midgut Neuroendocrine Tumors. *N. Engl. J. Med.* **2017**, *376*, 125−135.
(50) Buchegger, F.; Perillo-Adamer, F.; Dupertuis, Y. M.; Bischof Delaloye, A. Auger Radiation Targeted into DNA: A Therapy Perspective. *Eur. J. Nucl. Med. Mol. Imaging* **2006**, *33*, 1352−1363.
(51) Lehenberger, S.; Barkhausen, C.; Cohrs, S.; Fischer, E.; Grünberg, J.; Hohn, A.; Köster, U.; Schibli, R.; Türler, A.; Zhernosekov, K. The Low-Energy β^- and Electron Emitter ^{161}Tb as an Alternative to ^{177}Lu for Targeted Radionuclide Therapy. *Nucl. Med. Biol.* **2011**, *38*, 917−924.
(52) Fonslet, J.; Lee, B. Q.; Tran, T. A.; Siragusa, M.; Jensen, M.; Kibédi, T.; Stuchbery, A. E.; Severin, G. W. ^{135}La as an Auger-Electron Emitter for Targeted Internal Radiotherapy. *Phys. Med. Biol.* **2018**, *63*, No. 015026.
(53) Kim, Y.-S.; Brechbiel, M. W. An Overview of Targeted Alpha Therapy. *Tumor Biol.* **2012**, *33*, 573−590.
(54) Dekempeneer, Y.; Keyaerts, M.; Krasniqi, A.; Puttemans, J.; Muyldermans, S.; Lahoutte, T.; D'huyvetter, M.; Devoogdt, N. Targeted Alpha Therapy Using Short-Lived Alpha-Particles and the Promise of Nanobodies as Targeting Vehicle. *Expert Opin. Biol. Ther.* **2016**, *16*, 1035−1047.
(55) Makvandi, M.; Dupis, E.; Engle, J. W.; Nortier, F. M.; Fassbender, M. E.; Simon, S.; Birnbaum, E. R.; Atcher, R. W.; John, K. D.; Rixe, O.; Norenberg, J. P. Alpha-Emitters and Targeted Alpha Therapy in Oncology: From Basic Science to Clinical Investigations. *Target. Oncol.* **2018**, *13*, 189−203.
(56) Kassis, A. I.; Adelstein, S. J. Radiobiologic Principles in Radionuclide Therapy. *J. Nucl. Med.* **2005**, *46*, 4S−12S.
(57) Sgouros, G. Alpha-Particles for Targeted Therapy. *Adv. Drug Delivery Rev.* **2008**, *60*, 1402−1406.
(58) Sgouros, G.; Roeske, J. C.; McDevitt, M. R.; Palm, S.; Allen, B. J.; Fisher, D. R.; Brill, A. B.; Song, H.; Howell, R. W.; Akabani, G. MIRD Pamphlet No. 22 (Abridged): Radiobiology and Dosimetry of α-Particle Emitters for Targeted Radionuclide Therapy. *J. Nucl. Med.* **2010**, *51*, 311−328.
(59) Raju, M. R.; Eisen, Y.; Carpenter, S.; Inkret, W. C. Radiobiology of α Particles: III. Cell Inactivation by α-Particle Traversals of the Cell Nucleus. *Radiat. Res.* **1991**, *128*, 204−209.
(60) Behr, T. M.; Béhé, M.; Stabin, M. G.; Wehrmann, E.; Apostolidis, C.; Molinet, R.; Strutz, F.; Fayyazi, A.; Wieland, E.; Gratz, S.; Koch, L.; Goldenberg, D. M.; Becker, W. High-Linear Energy Transfer (LET) α *versus* Low-LET β Emitters in Radioimmunotherapy of Solid Tumors: Therapeutic Efficacy and Dose-Limiting Toxicity of ^{213}Bi- *versus* ^{90}Y-Labeled CO17−1A Fab' Fragments in a Human Colonic Cancer Model. *Cancer Res.* **1999**, *59*, 2635−2643.
(61) Graf, F.; Fahrer, J.; Maus, S.; Morgenstern, A.; Bruchertseifer, F.; Venkatachalam, S.; Fottner, C.; Weber, M. M.; Huelsenbeck, J.; Schreckenberger, M.; Kaina, B.; Miederer, M. DNA Double Strand Breaks as Predictor of Efficacy of the Alpha-Particle Emitter Ac-225 and the Electron Emitter Lu-177 for Somatostatin Receptor Targeted Radiotherapy. *PLoS One* **2014**, *9*, No. e88239.

DOI: 10.1021/acs.inorgchem.9b01277
Inorg. Chem. XXXX, XXX, XXX−XXX

(62) Allen, B. J.; Blagojevic, N. Alpha- and Beta-Emitting Radiolanthanides in Targeted Cancer Therapy: The Potential Role of Terbium-149. *Nucl. Med. Commun.* **1996**, *17*, 40−47.
(63) Beyer, G.-J.; Miederer, M.; Vranješ-Đurić, S.; Čomor, J. J.; Künzi, G.; Hartley, O.; Senekowitsch-Schmidtke, R.; Soloviev, D.; Buchegger, F. Targeted Alpha Therapy in Vivo: Direct Evidence for Single Cancer Cell Kill Using ^{149}Tb-Rituximab. *Eur. J. Nucl. Med. Mol. Imaging* **2004**, *31*, 547−554.
(64) Geerlings, M. W.; Kaspersen, F. M.; Apostolidis, C.; van der Hout, R. The Feasibility of ^{225}Ac as a Source of Alpha-Particles in Radioimmunotherapy. *Nucl. Med. Commun.* **1993**, *14*, 121−125.
(65) Miederer, M.; Scheinberg, D. A.; McDevitt, M. R. Realizing the Potential of the Actinium-225 Radionuclide Generator in Targeted Alpha Particle Therapy Applications. *Adv. Drug Delivery Rev.* **2008**, *60*, 1371−1382.
(66) Thiele, N. A.; Wilson, J. J. Actinium-225 for Targeted α Therapy: Coordination Chemistry and Current Chelation Approaches. *Cancer Biother. Radiopharm.* **2018**, *33*, 336−348.
(67) Morgenstern, A.; Apostolidis, C.; Kratochwil, C.; Sathekge, M.; Krolicki, L.; Bruchertseifer, F. An Overview of Targeted Alpha Therapy with ^{225}Actinium and ^{213}Bismuth. *Curr. Radiopharm.* **2018**, *11*, 200−208.
(68) Henriksen, G.; Bruland, Ø. S.; Larsen, R. H. Thorium and Actinium Polyphosphonate Compounds As Bone-Seeking Alpha Particle-Emitting Agents. *Anticancer Res.* **2004**, *24*, 101−105.
(69) Dahle, J.; Borrebæk, J.; Jonasdottir, T. J.; Hjelmerud, A. K.; Melhus, K. B.; Bruland, Ø. S.; Press, O. W.; Larsen, R. H. Targeted Cancer Therapy with a Novel Low-Dose Rate α-Emitting Radioimmunoconjugate. *Blood* **2007**, *110*, 2049−2056.
(70) Dahle, J.; Larsen, R. H. Targeted Alpha-Particle Therapy with ^{227}Th-Labeled Antibodies. *Curr. Radiopharm.* **2008**, *1*, 209−214.
(71) Dahle, J.; Krogh, C.; Melhus, K. B.; Borrebæk, J.; Larsen, R. H.; Kvinnsland, Y. *In Vitro* Cytotoxicity of Low-Dose-Rate Radioimmunotherapy by the Alpha-Emitting Radioimmunoconjugate Thorium-227-DOTA-Rituximab. *Int. J. Radiat. Oncol., Biol., Phys.* **2009**, *75*, 886−895.
(72) Abbas, N.; Heyerdahl, H.; Bruland, Ø. S.; Borrebæk, J.; Nesland, J.; Dahle, J. Experimental α-Particle Radioimmunotherapy of Breast Cancer Using ^{227}Th-Labeled p-Benzyl-DOTA-Trastuzumab. *EJNMMI Res.* **2011**, *1*, 18.
(73) Ramdahl, T.; Bonge-Hansen, H. T.; Ryan, O. B.; Larsen, Å.; Herstad, G.; Sandberg, M.; Bjerke, R. M.; Grant, D.; Brevik, E. M.; Cuthbertson, A. S. An Efficient Chelator for Complexation of Thorium-227. *Bioorg. Med. Chem. Lett.* **2016**, *26*, 4318−4321.
(74) Hagemann, U. B.; Mihaylova, D.; Uran, S. R.; Borrebaek, J.; Grant, D.; Bjerke, R. M.; Karlsson, J.; Cuthbertson, A. S. Targeted Alpha Therapy Using a Novel CD70 Targeted Thorium-227 Conjugate in in Vitro and in Vivo Models of Renal Cell Carcinoma. *Oncotarget* **2017**, *8*, 56311−56326.
(75) Deblonde, G. J.-P.; Lohrey, T. D.; Booth, C. H.; Carter, K. P.; Parker, B. F.; Larsen, Å.; Smeets, R.; Ryan, O. B.; Cuthbertson, A. S.; Abergel, R. J. Solution Thermodynamics and Kinetics of Metal Complexation with a Hydroxypyridinone Chelator Designed for Thorium-227 Targeted Alpha Therapy. *Inorg. Chem.* **2018**, *57*, 14337−14346.
(76) Wickstroem, K.; Hagemann, U. B.; Cruciani, V.; Wengner, A. M.; Kristian, A.; Ellingsen, C.; Siemeister, G.; Bjerke, R. M.; Karlsson, J.; Ryan, O. B.; Linden, L.; Mumberg, D.; Ziegelbauer, K.; Cuthbertson, A. S. Synergistic Effect of a Mesothelin Targeted Thorium-227 Conjugate in Combination with DNA Damage Response Inhibitors in Ovarian Cancer Xenograft Models. *J. Nucl. Med.* **2019**, DOI: 10.2967/jnumed.118.223701.
(77) Kratochwil, C.; Bruchertseifer, F.; Giesel, F. L.; Weis, M.; Verburg, F. A.; Mottaghy, F.; Kopka, K.; Apostolidis, C.; Haberkorn, U.; Morgenstern, A. ^{225}Ac-PSMA-617 for PSMA-Targeted α-Radiation Therapy of Metastatic Castration-Resistant Prostate Cancer. *J. Nucl. Med.* **2016**, *57*, 1941−1944.
(78) Kratochwil, C.; Bruchertseifer, F.; Rathke, H.; Bronzel, M.; Apostolidis, C.; Weichert, W.; Haberkorn, U.; Giesel, F. L.; Morgenstern, A. Targeted α-Therapy of Metastatic Castration-Resistant Prostate Cancer with ^{225}Ac-PSMA-617: Dosimetry Estimate and Empirical Dose Finding. *J. Nucl. Med.* **2017**, *58*, 1624−1631.
(79) Study to evaluate the safety, tolerability, pharmacokinetics, and anti-tumor activity of a thorium-227 labeled antibody-chelator conjugate, in patients with metastatic castration resistant prostate cancer (NCT03724747). https://clinicaltrials.gov/ct2/show/NCT03724747?term=thorium&rank=1 (accessed Apr 27, 2019).
(80) Jurcic, J. G.; Rosenblat, T. L.; McDevitt, M. R.; Pandit-Taskar, N.; Carrasquillo, J. A.; Chanel, S. M.; Zikaras, K.; Frattini, M. G.; Maslak, P. M.; Cicic, D.; Larson, S. M.; Scheinberg, D. A. Targeted Alpha-Particle Nano-Generator Actinium-225 (^{225}Ac)-Lintuzumab (Anti-CD33) in Acute Myeloid Leukemia (AML). *Clin. Lymphoma, Myeloma Leuk.* **2013**, *13*, S379−S380.
(81) Jurcic, J. G.; Ravandi, F.; Pagel, J. M.; Park, J. H.; Smith, B. D.; Douer, D.; Levy, M. Y.; Estey, E.; Kantarjian, H. M.; Earle, D.; Cicic, D.; Scheinberg, D. A. Phase I Trial of α-Particle Therapy with Actinium-225 (^{225}Ac)-Lintuzumab (Anti-CD33) and Low-Dose Cytarabine (LDAC) in Older Patients with Untreated Acute Myeloid Leukemia (AML). *J. Clin. Oncol.* **2015**, *33*, 7050.
(82) Kratochwil, C.; Bruchertseifer, F.; Giesel, F.; Apostolidis, C.; Haberkorn, U.; Morgenstern, A. Ac-225-DOTATOC - an Empiric Dose Finding for Alpha Particle Emitter Based Radionuclide Therapy of Neuroendocrine Tumors. *J. Nucl. Med.* **2015**, *56*, 1232.
(83) First-in-human study of BAY2287411 injection, a thorium-227 labeled antibody-chelator conjugate, in patients with tumors known to express mesothelin. (NCT03507452) https://clinicaltrials.gov/ct2/show/NCT03507452?term=thorium&rank=2 (accessed Apr 27, 2019).
(84) Morgenstern, A.; Lebeda, O.; Stursa, J.; Bruchertseifer, F.; Capote, R.; McGinley, J.; Rasmussen, G.; Sin, M.; Zielinska, B.; Apostolidis, C. Production of ^{230}U/^{226}Th for Targeted Alpha Therapy via Proton Irradiation of ^{231}Pa. *Anal. Chem.* **2008**, *80*, 8763−8770.
(85) Montavon, G.; Repinc, U.; Apostolidis, C.; Bruchertseifer, F.; Abbas, K.; Morgenstern, A. Investigation of Para-Sulfonatocalix[n]-Arenes [n = 6, 8] as Potential Chelates for ^{230}U. *Dalton Trans.* **2010**, *39*, 1366−1374.
(86) Ghiorso, A.; Thompson, S. G.; Higgins, G. H.; Seaborg, G. T.; Studier, M. H.; Fields, P. R.; Fried, S. M.; Diamond, H.; Mech, J. F.; Pyle, G. L.; Huizenga, J. R.; Hirsch, A.; Manning, W. M.; Browne, C. I.; Smith, H. L.; Spence, R. W. New Elements Einsteinium and Fermium, Atomic Numbers 99 and 100. *Phys. Rev.* **1955**, *99*, 1048−1049.
(87) Fields, P. R.; Studier, M. H.; Diamond, H.; Mech, J. F.; Inghram, M. G.; Pyle, G. L.; Stevens, C. M.; Fried, S.; Manning, W. M.; Ghiorso, A.; Thompson, S. G.; Higgins, G. H.; Seaborg, G. T. Transplutonium Elements in Thermonuclear Test Debris. *Phys. Rev.* **1956**, *102*, 180−182.
(88) Wilbur, D. S. Chemical and Radiochemical Considerations in Radiolabeling with α-Emitting Radionuclides. *Curr. Radiopharm.* **2011**, *4*, 214−247.
(89) Schlea, C. S.; Stoddard, D. H. Californium Isotopes Proposed for Intracavity and Interstitial Radiation Therapy with Neutrons. *Nature* **1965**, *206*, 1058−1059.
(90) Wang, C.-K. C. Progress in Californium-252 Neutron Brachytherapy. In *Brachytherapy*; Kishi, K., Ed.; InTech: Rijeka, Croatia, 2012; pp 33−58.
(91) Pelvic external combined with 252-Cf neutron intracavitary radiotherapy with or without platinum in treating advanced cervical cancer. (NCT02835404) https://clinicaltrials.gov/ct2/show/NCT02835404?term=252cf&rank=1 (accessed Jun 6, 2019).
(92) Price, E. W.; Orvig, C. Matching Chelators to Radiometals for Radiopharmaceuticals. *Chem. Soc. Rev.* **2014**, *43*, 260−290.
(93) Cacheris, W. P.; Nickle, S. K.; Sherry, A. D. Thermodynamic Study of Lanthanide Complexes of 1,4,7-Triazacyclononane-*N*,*N*′,*N*″-Triacetic Acid and 1,4,7,10-Tetraazacyclododecane-*N*,*N*′,*N*″,*N*‴-Tetraacetic Acid. *Inorg. Chem.* **1987**, *26*, 958−960.
(94) Loncin, M. F.; Desreux, J. F.; Merciny, E. Coordination of Lanthanides by Two Polyamino Polycarboxylic Macrocycles:

DOI: 10.1021/acs.inorgchem.9b01277
Inorg. Chem. XXXX, XXX, XXX−XXX

Formation of Highly Stable Lanthanide Complexes. *Inorg. Chem.* **1986**, *25*, 2646−2648.
(95) Clarke, E. T.; Martell, A. E. Stabilities of Trivalent Metal Ion Complexes of the Tetraacetate Derivatives of 12-, 13- and 14-Membered Tetraazamacrocycles. *Inorg. Chim. Acta* **1991**, *190*, 37−46.
(96) Wu, S. L.; Horrocks, W. D. Direct Determination of Stability Constants of Lanthanide Ion Chelates by Laser-Excited Europium(III) Luminescence Spectroscopy: Application to Cyclic and Acyclic Aminocarboxylate Complexes. *J. Chem. Soc., Dalton Trans.* **1997**, 1497−1502.
(97) Thiele, N. A.; Brown, V.; Kelly, J. M.; Amor-Coarasa, A.; Jermilova, U.; MacMillan, S. N.; Nikolopoulou, A.; Ponnala, S.; Ramogida, C. F.; Robertson, A. K. H.; Rodríguez-Rodríguez, C.; Schaffer, P.; Williams, C., Jr.; Babich, J. W.; Radchenko, V.; Wilson, J. J. An Eighteen-Membered Macrocyclic Ligand for Actinium-225 Targeted Alpha Therapy. *Angew. Chem., Int. Ed.* **2017**, *56*, 14712−14717.
(98) Thiele, N. A.; MacMillan, S. N.; Wilson, J. J. Rapid Dissolution of $BaSO_4$ by Macropa, an 18-Membered Macrocycle with High Affinity for Ba^{2+}. *J. Am. Chem. Soc.* **2018**, *140*, 17071−17078.
(99) Chang, C. A.; Rowland, M. E. Metal Complex Formation with 1,10-Diaza-4,7,13,16-Tetraoxacyclooctadecane-*N*,*N*′-Diacetic Acid. An Approach to Potential Lanthanide Ion Selective Reagents. *Inorg. Chem.* **1983**, *22*, 3866−3869.
(100) Hancock, R. D.; Bhavan, R.; Shaikjee, M. S.; Wade, P. W.; Hearn, A. The Metal Ion Size-Dependent Pattern of Stabilization Produced by Adding Alcoholic or Ethereal Oxygen Donors to Ligands. *Inorg. Chim. Acta* **1986**, *112*, L23−L25.
(101) Damu, K. V.; Shaikjee, M. S.; Michael, J. P.; Howard, A. S.; Hancock, R. D. Control of Metal Ion Selectivity in Ligands Containing Neutral Oxygen and Pyridyl Groups. *Inorg. Chem.* **1986**, *25*, 3879−3883.
(102) Hancock, R. D.; Bhavan, R.; Wade, P. W.; Boeyens, J. C. A.; Dobson, S. M. Ligand Design for Complexation in Aqueous Solution. 1. Neutral Oxygen Donor Bearing Groups as a Means of Controlling Size-Based Selectivity for Metal Ions. *Inorg. Chem.* **1989**, *28*, 187−194.
(103) Brücher, E.; Györi, B.; Emri, J.; Solymosi, P.; Sztanyik, L. B.; Varga, L. 1,10-Diaza-4,7,13,16-Tetraoxacyclooctadecane-1,10-Bis(Malonate), a Ligand with High Sr^{2+}/Ca^{2+} and Pb^{2+}/Zn^{2+} Selectivities in Aqueous Solution. *J. Chem. Soc., Chem. Commun.* **1993**, 574−575.
(104) Zhang, X. X.; Bordunov, A. V.; Bradshaw, J. S.; Dalley, N. K.; Kou, X.; Izatt, R. M. A New Highly Selective Macrocycle for K^+ and Ba^{2+}: Effect of Formation of Pseudo Second Macroring through Complexation. *J. Am. Chem. Soc.* **1995**, *117*, 11507−11511.
(105) Bordunov, A. V.; Bradshaw, J. S.; Zhang, X. X.; Dalley, N. K.; Kou, X.; Izatt, R. M. Synthesis and Properties of 5-Chloro-8-Hydroxyquinoline-Substituted Azacrown Ethers: A New Family of Highly Metal Ion-Selective Lariat Ethers. *Inorg. Chem.* **1996**, *35*, 7229−7240.
(106) Su, N.; Bradshaw, J. S.; Zhang, X. X.; Song, H.; Savage, P. B.; Xue, G.; Krakowiak, K. E.; Izatt, R. M. Syntheses and Metal Ion Complexation of Novel 8-Hydroxyquinoline-Containing Diaza-18-Crown-6 Ligands and Analogues. *J. Org. Chem.* **1999**, *64*, 8855−8861.
(107) Jensen, M. P.; Chiarizia, R.; Shkrob, I. A.; Ulicki, J. S.; Spindler, B. D.; Murphy, D. J.; Hossain, M.; Roca-Sabio, A.; Platas-Iglesias, C.; de Blas, A.; Rodríguez-Blas, T. Aqueous Complexes for Efficient Size-Based Separation of Americium from Curium. *Inorg. Chem.* **2014**, *53*, 6003−6012.
(108) Regueiro-Figueroa, M.; Barriada, J. L.; Pallier, A.; Esteban-Gómez, D.; De Blas, A.; Rodríguez-Blas, T.; Tóth, É.; Platas-Iglesias, C. Stabilizing Divalent Europium in Aqueous Solution Using Size-Discrimination and Electrostatic Effects. *Inorg. Chem.* **2015**, *54*, 4940−4952.
(109) Kelly, J. M.; Amor-Coarasa, A.; Ponnala, S.; Nikolopoulou, A.; Williams, C.; Thiele, N. A.; Schyler, D.; Wilson, J. J.; DiMagno, S. G.; Babich, J. W. A Single Dose of ^{225}Ac-RPS-074 Induces a Complete Tumor Response in a LNCaP Xenograft Model. *J. Nucl. Med.* **2019**, *60*, 649−655.
(110) Roca-Sabio, A.; Mato-Iglesias, M.; Esteban-Gómez, D.; Tóth, É.; de Blas, A.; Platas-Iglesias, C.; Rodríguez-Blas, T. Macrocyclic Receptor Exhibiting Unprecedented Selectivity for Light Lanthanides. *J. Am. Chem. Soc.* **2009**, *131*, 3331−3341.
(111) Ferreirós-Martínez, R.; Esteban-Gómez, D.; Tóth, É.; de Blas, A.; Platas-Iglesias, C.; Rodríguez-Blas, T. Macrocyclic Receptor Showing Extremely High Sr(II)/Ca(II) and Pb(II)/Ca(II) Selectivities with Potential Application in Chelation Treatment of Metal Intoxication. *Inorg. Chem.* **2011**, *50*, 3772−3784.
(112) Landini, D.; Montanari, F.; Rolla, F. Phase-Transfer Catalysts: Synthesis and Catalytic Activity of a Tricyclohexyl[2.2.2]Cryptand (Perhydro-Tribenzohexaoxadiaza[8.8.8]Eicosane. *Synthesis* **1978**, *3*, 223−225.
(113) Lin, W. O.; de Souza, M. C. B. V.; Alt, H. G. Synthesis, Characterization and Complexation Studies with K^+ and Ca^{2+} Cations of Trans-1.2-Cyclohexanedioxydiacetamides. *Z. Naturforsch.* **1988**, *43*, 165−170.
(114) Hancock, R. D.; Martell, A. E. Ligand Design for Selective Complexation of Metal Ions in Aqueous Solution. *Chem. Rev.* **1989**, *89*, 1875−1914.
(115) Martell, A. E.; Hancock, R. D.; Motekaitis, R. J. Factors Affecting Stabilities of Chelate, Macrocyclic and Macrobicyclic Complexes in Solution. *Coord. Chem. Rev.* **1994**, *133*, 39−65.
(116) Smith, R. M.; Martell, A. E. Critical Stability Constants, Enthalpies and Entropies for the Formation of Metal Complexes of Aminopolycarboxylic Acids and Carboxylic Acids. *Sci. Total Environ.* **1987**, *64*, 125−147.
(117) Kelley, M. P.; Bessen, N. P.; Su, J.; Urban, M.; Sinkov, S. I.; Lumetta, G. J.; Batista, E. R.; Yang, P.; Shafer, J. C. Revisiting Complexation Thermodynamics of Transplutonium Elements up to Einsteinium. *Chem. Commun.* **2018**, *54*, 10578−10581.
(118) Martell, A. E.; Hancock, R. D. *Metal Complexes in Aqueous Solutions*; Plenum Press: New York, 1996.
(119) Izatt, R. M.; Pawlak, K.; Bradshaw, J. S.; Bruening, R. L. Thermodynamic and Kinetic Data for Macrocycle Interaction with Cations and Anions. *Chem. Rev.* **1991**, *91*, 1721−2085.
(120) Hubin, T. J. Synthesis and Coordination Chemistry of Topologically Constrained Azamacrocycles. *Coord. Chem. Rev.* **2003**, *241*, 27−46.
(121) Cox, B. G.; Firman, P.; Schneider, I.; Schneider, H. Rates and Equilibria of Alkaline-Earth-Metal Complexes with Diaza Crown Ethers in Methanol. *Inorg. Chem.* **1988**, *27*, 4018−4021.
(122) de Sousa, A. S.; Croft, G. J. B.; Wagner, C. A.; Michael, J. P.; Hancock, R. D. Effect of Cyclohexylene Bridges on the Metal Ion Size Based Selectivity of Ligands in Aqueous Solution. *Inorg. Chem.* **1991**, *30*, 3525−3529.
(123) Bradshaw, J. S.; Krakowiak, K. E.; Huszthy, P.; Izatt, R. M. Proton-Ionizable Crown Compounds. 20. The Synthesis of Polyazatriazolo-, Polyazabistriazolo- and Bispyridono-Crown Ligands Containing Lipophilic Hydrocarbon Substituents. *J. Heterocycl. Chem.* **1991**, *28*, 773−775.
(124) Elshani, S.; Apgar, P.; Wang, S.; Wai, C. M. New Proton-Ionizable Macrocyclic Compounds Containing One and Two Triazole Subcyclic Units — Synthesis and Complexation Properties. *J. Heterocycl. Chem.* **1994**, *31*, 1271−1274.
(125) Caiazza, D.; Lincoln, S. F.; Ward, A. D. A Preparative Study of Some Coronands and Their Complexation of Silver(I), Zinc(II), Cadmium(II) and Lead(II). *Inorg. Chim. Acta* **2004**, *357*, 716−722.
(126) Doble, D. M. J.; Melchior, M.; O'Sullivan, B.; Siering, C.; Xu, J.; Pierre, V. C.; Raymond, K. N. Toward Optimized High-Relaxivity MRI Agents: The Effect of Ligand Basicity on the Thermodynamic Stability of Hexadentate Hydroxypyridonate/Catecholate Gadolinium(III) Complexes. *Inorg. Chem.* **2003**, *42*, 4930−4937.
(127) Jensen, K. A. Tentative Proposals for Nomenclature of Absolute Configurations Concerned with Six-Coordinated Complexes Based on the Octahedron. *Inorg. Chem.* **1970**, *9*, 1−5.
(128) Hancock, R. D.; Evers, A.; Ngwenya, M. P.; Wade, P. W. Structurally Reinforced Macrocyclic Ligands That Show Greatly Enhanced Selectivity for Metal Ions on the Basis of the Match in Size

DOI: 10.1021/acs.inorgchem.9b01277
Inorg. Chem. XXXX, XXX, XXX−XXX

between the Metal Ion and the Macrocyclic Cavity. *J. Chem. Soc., Chem. Commun.* **1987**, 1129−1130.
(129) Hancock, R. D.; Pattrick, G.; Wade, P. W.; Hosken, G. D. Structurally Reinforced Macrocyclic Ligands. *Pure Appl. Chem.* **1993**, *65*, 473−476.
(130) Roca-Sabio, A.; Regueiro-Figueroa, M.; Esteban-Gómez, D.; de Blas, A.; Rodríguez-Blas, T.; Platas-Iglesias, C. Density Functional Dependence of Molecular Geometries in Lanthanide(III) Complexes Relevant to Bioanalytical and Biomedical Applications. *Comput. Theor. Chem.* **2012**, *999*, 93−104.
(131) Regueiro-Figueroa, M.; Esteban-Gõmez, D.; De Blas, A.; Rodríguez-Blas, T.; Platas-Iglesias, C. Understanding Stability Trends along the Lanthanide Series. *Chem. - Eur. J.* **2014**, *20*, 3974−3981.
(132) Bryantsev, V. S.; Diallo, M. S.; Goddard, W. A. Calculation of Solvation Free Energies of Charged Solutes Using Mixed Cluster/Continuum Models. *J. Phys. Chem. B* **2008**, *112*, 9709−9719.
(133) Vukovic, S.; Hay, B. P.; Bryantsev, V. S. Predicting Stability Constants for Uranyl Complexes Using Density Functional Theory. *Inorg. Chem.* **2015**, *54*, 3995−4001.
(134) Ivanov, A. S.; Bryantsev, V. S. A Computational Approach to Predicting Ligand Selectivity for the Size-Based Separation of Trivalent Lanthanides. *Eur. J. Inorg. Chem.* **2016**, *2016*, 3474−3479.
(135) Cosentino, U.; Villa, A.; Pitea, D.; Moro, G.; Barone, V. Extension of Computational Chemistry to the Study of Lanthanide-(III) Ions in Aqueous Solution: Implementation and Validation of a Continuum Solvent Approach. *J. Phys. Chem. B* **2000**, *104*, 8001−8007.
(136) Buist, D.; Williams, N. J.; Reibenspies, J. H.; Hancock, R. D. Control of Metal Ion Size-Based Selectivity through Chelate Ring Geometry. Metal Ion Complexing Properties of 2,2′-Biimidazole. *Inorg. Chem.* **2010**, *49*, 5033−5039.
(137) Wilson, J. J.; Ferrier, M.; Radchenko, V.; Maassen, J. R.; Engle, J. W.; Batista, E. R.; Martin, R. L.; Nortier, F. M.; Fassbender, M. E.; John, K. D.; Birnbaum, E. R. Evaluation of Nitrogen-Rich Macrocyclic Ligands for the Chelation of Therapeutic Bismuth Radioisotopes. *Nucl. Med. Biol.* **2015**, *42*, 428−438.
(138) Martell, A. E.; Smith, R. M. *Critical Stability Constants*; Plenum Press: New York, 1974; Vol. *1*.
(139) Brechbiel, M. W.; Pippin, C. G.; McMurry, T. J.; Milenic, D.; Roselli, M.; Colcher, D.; Gansow, O. A. An Effective Chelating Agent for Labelling of Monoclonal Antibody with ^{212}Bi for α-Particle Mediated Radioimmunotherapy. *J. Chem. Soc., Chem. Commun.* **1991**, 1169−1170.
(140) Camera, L.; Kinuya, S.; Garmestani, K.; Wu, C.; Brechbiel, M. W.; Pai, L. H.; McMurry, T. J.; Gansow, O. A.; Pastan, I.; Paik, C. H.; Carrasquillo, J. A. Evaluation of the Serum Stability and In Vivo Biodistribution of CHX-DTPA and Other Ligands for Yttrium Labeling of Monoclonal Antibodies. *J. Nucl. Med.* **1994**, *35*, 882−889.
(141) Wu, C.; Kobayashi, H.; Sun, B.; Yoo, T. M.; Paik, C. H.; Gansow, O. A.; Carrasquillo, J. A.; Pastan, I.; Brechbiel, M. W. Stereochemical Influence on the Stability of Radio-Metal Complexes in Vivo. Synthesis and Evaluation of the Four Stereoisomers of 2-(p-Nitrobenzyl)-Trans-CyDTPA. *Bioorg. Med. Chem.* **1997**, *5*, 1925−1934.
(142) Ramogida, C. F.; Cawthray, J. F.; Boros, E.; Ferreira, C. L.; Patrick, B. O.; Adam, M. J.; Orvig, C. H_2*CHX* Dedpa and H_4*CHX* Octapa—Chiral Acyclic Chelating Ligands for $^{67/68}$Ga and ^{111}In Radiopharmaceuticals. *Inorg. Chem.* **2015**, *54*, 2017−2031.
(143) Mato-Iglesias, M.; Roca-Sabio, A.; Pálinkás, Z.; Esteban-Gómez, D.; Platas-Iglesias, C.; Tóth, É.; de Blas, A.; Rodríguez-Blas, T. Lanthanide Complexes Based on a 1,7-Diaza-12-Crown-4 Platform Containing Picolinate Pendants: A New Structural Entry for the Design of Magnetic Resonance Imaging Contrast Agents. *Inorg. Chem.* **2008**, *47*, 7840−7851.
(144) Zeng, X.; Coquiére, D.; Alenda, A.; Garrier, E.; Prangé, T.; Li, Y.; Reinaud, O.; Jabin, I. Efficient Synthesis of Calix[6]Tmpa: A New Calix[6]Azacryptand with Unique Conformational and Host-Guest Properties. *Chem. - Eur. J.* **2006**, *12*, 6393−6402.
(145) Dietrich, B.; Lehn, J. M.; Sauvage, J. P.; Blanzat, J. Cryptates-X. Syntheses et Proprietes Physiques de Systemes Diaza-Polyoxa-Macrobicycliques. *Tetrahedron* **1973**, *29*, 1629−1645.
(146) Sheldrick, G. M. SHELXT - Integrated Space-Group and Crystal-Structure Determination. *Acta Crystallogr., Sect. A: Found. Adv.* **2015**, *71*, 3−8.
(147) Sheldrick, G. M. A Short History of SHELX. *Acta Crystallogr., Sect. A: Found. Crystallogr.* **2008**, *64*, 112−122.
(148) Müller, P. Practical Suggestions for Better Crystal Structures. *Crystallogr. Rev.* **2009**, *15*, 57−83.
(149) Dolomanov, O. V.; Bourhis, L. J.; Gildea, R. J.; Howard, J. A. K.; Puschmann, H. OLEX2: A Complete Structure Solution, Refinement and Analysis Program. *J. Appl. Crystallogr.* **2009**, *42*, 339−341.
(150) Suntharalingam, K.; Johnstone, T. C.; Bruno, P. M.; Lin, W.; Hemann, M. T.; Lippard, S. J. Bidentate Ligands on Osmium(VI) Nitrido Complexes Control Intracellular Targeting and Cell Death Pathways. *J. Am. Chem. Soc.* **2013**, *135*, 14060−14063.
(151) Gans, P.; O'Sullivan, B. GLEE, a New Computer Program for Glass Electrode Calibration. *Talanta* **2000**, *51*, 33−37.
(152) Sweeton, F. H.; Mesmer, R. E.; Baes, C. F. Acidity Measurements at Elevated Temperatures. VII. Dissociation of Water. *J. Solution Chem.* **1974**, *3*, 191−214.
(153) Gans, P.; Sabatini, A.; Vacca, A. Investigation of Equilibria in Solution. Determination of Equilibrium Constants with the HYPERQUAD Suite of Programs. *Talanta* **1996**, *43*, 1739−1753.
(154) Baes, C. F.; Mesmer, R. E. *The Hydrolysis of Cations*; Wiley: New York, 1976.
(155) Frisch, M. J.; Trucks, G. W.; Schlegel, H. B.; Scuseria, G. E.; Robb, M. A.; Cheeseman, J. R.; Scalmani, G.; Barone, V.; Mennucci, B.; Petersson, G. A.; Nakatsuji, H.; Caricato, M.; Li, X.; Hratchian, H. P.; Izmaylov, A. F.; Bloino, J.; Zheng, G.; Sonnenberg, J. L.; Hada, M.; Ehara, M.; Toyota, K.; Fukuda, R.; Hasegawa, J.; Ishida, M.; Nakajima, T.; Honda, Y.; Kitao, O.; Nakai, H.; Vreven, T.; Montgomery, J. A., Jr.; Peralta, J. E.; Ogliaro, F.; Bearpark, M.; Heyd, J. J.; Brothers, E.; Kudin, K. N.; Staroverov, V. N.; Kobayashi, R.; Normand, J.; Raghavachari, K.; Rendell, A.; Burant, J. C.; Iyengar, S. S.; Tomasi, J.; Cossi, M.; Rega, N.; Millam, N. J.; Klene, M.; Knox, J. E.; Cross, J. B.; Bakken, V.; Adamo, C.; Jaramillo, J.; Gomperts, R.; Stratmann, R. E.; Yazyev, O.; Austin, A. J.; Cammi, R.; Pomelli, C.; Ochterski, J. W.; Martin, R. L.; Morokuma, K.; Zakrzewski, V. G.; Voth, G. A.; Salvador, P.; Dannenberg, J. J.; Dapprich, S.; Daniels, A. D.; Farkas, Ö.; Foresman, J. B.; Ortiz, J. V.; Cioslowski, J.; Fox, D. J. *Gaussian09*, revision A.02; Gaussian Inc.: Wallingford, CT, 2009.
(156) Ellis, R. J.; Brigham, D. M.; Delmau, L.; Ivanov, A. S.; Williams, N. J.; Vo, M. N.; Reinhart, B.; Moyer, B. A.; Bryantsev, V. S. "Straining" to Separate the Rare Earths: How the Lanthanide Contraction Impacts Chelation by Diglycolamide Ligands. *Inorg. Chem.* **2017**, *56*, 1152−1160.
(157) Tao, J.; Perdew, J. P.; Staroverov, V. N.; Scuseria, G. E. Climbing the Density Functional Ladder: Nonempirical Meta−Generalized Gradient Approximation Designed for Molecules and Solids. *Phys. Rev. Lett.* **2003**, *91*, 146401.
(158) Dolg, M.; Stoll, H.; Savin, A.; Preuss, H. Energy-Adjusted Pseudopotentials for the Rare Earth Elements. *Theor. Chim. Acta* **1989**, *75*, 173−194.
(159) Dolg, M.; Stoll, H.; Preuss, H. A Combination of Quasirelativistic Pseudopotential and Ligand Field Calculations for Lanthanoid Compounds. *Theor. Chim. Acta* **1993**, *85*, 441−450.
(160) Maron, L.; Eisenstein, O. Do f Electrons Play a Role in the Lanthanide−Ligand Bonds? A DFT Study of $Ln(NR_2)_3$; R = H, SiH_3. *J. Phys. Chem. A* **2000**, *104*, 7140−7143.
(161) Esteban-Gomez, D.; Roca-Sabio, A.; Platas-Iglesias, C.; de Blas, A.; Rodriguez-Blas, T.; Regueiro-Figueroa, M. Applications of Density Functional Theory (DFT) to Investigate the Structural, Spectroscopic and Magnetic Properties of Lanthanide(III) Complexes. *Curr. Inorg. Chem.* **2011**, *1*, 91−116.

DOI: 10.1021/acs.inorgchem.9b01277
Inorg. Chem. XXXX, XXX, XXX−XXX

(162) Eisenstein, O.; Maron, L. DFT Studies of Some Structures and Reactions of Lanthanides Complexes. *J. Organomet. Chem.* **2002**, *647*, 190−197.
(163) Marenich, A. V.; Cramer, C. J.; Truhlar, D. G. Universal Solvation Model Based on Solute Electron Density and on a Continuum Model of the Solvent Defined by the Bulk Dielectric Constant and Atomic Surface Tensions. *J. Phys. Chem. B* **2009**, *113*, 6378−6396.
(164) Zawada, A.; Góra, R. W.; Mikołajczyk, M. M.; Bartkowiak, W. On the Calculations of Interaction Energies and Induced Electric Properties within the Polarizable Continuum Model. *J. Phys. Chem. A* **2012**, *116*, 4409−4416.
(165) Boys, S. F.; Bernardi, F. The Calculation of Small Molecular Interactions by the Differences of Separate Total Energies. Some Procedures with Reduced Errors. *Mol. Phys.* **1970**, *19*, 553−566.

DOI: 10.1021/acs.inorgchem.9b01277
Inorg. Chem. XXXX, XXX, XXX−XXX